











ARTICLE

TRAF3–EWSR1 signaling axis acts as a checkpoint on germinal center responses

Yanchuan Li¹ , Lele Zhu² , Chun-Jung Ko³ , Jin-Young Yang⁴ , Hongjiao Wang⁵ , Ganiraju Manyam⁶ , Jing Wang⁶ , Xuhong Cheng⁷ , Shuli Zhao⁸ , and Zuliang Jie⁵ 

The formation of germinal centers (GCs) is crucial for humoral immunity and vaccine efficacy. Constant stimulation through microbiota drives the formation of constitutive GCs in Peyer’s patches (PPs), which generate B cells that produce antibodies against gut antigens derived from commensal bacteria and infectious pathogens. However, the molecular mechanism that regulates this persistent process is poorly understood. We report that Ewing Sarcoma Breakpoint Region 1 (EWSR1) is a brake to constitutive GC generation and immunoglobulin G (IgG) production in PPs, vaccination-induced GC formation, and IgG responses. Mechanistically, EWSR1 suppresses Bcl6 upregulation after antigen encounter, thereby negatively regulating induced GC B cell generation and IgG production. We further showed that tumor necrosis factor receptor-associated factor (TRAF) 3 serves as a negative regulator of EWSR1. These results established that the TRAF3–EWSR1 signaling axis acts as a checkpoint for Bcl6 expression and GC responses, indicating that this axis is a therapeutic target to tune GC responses and humoral immunity in infectious diseases.

Introduction

Immune responses to protein antigens involve the formation of germinal centers (GCs) within B cell follicles of secondary lymphoid tissues, wherein activated B cells undergo clonal expansion and a series of complex and dynamic processes to differentiate into antibody-secreting plasma cells and memory B cells (Victoria and Nussenzweig, 2022; Young and Brink, 2021). Successful vaccines or natural immune protection induces robust and prolonged GC reactions that are pivotal for generating high-affinity and durable antibody responses. Indeed, a better GC response leading to high levels of neutralizing antibodies may represent a better protective efficacy against most infectious diseases. Thus, studying the formation of GCs has the potential to provide novel insights into the molecular mechanism of B cell fate determination, which assists the development of vaccines or therapies for challenging or emerging pathogens, such as SARS-CoV-2 (Turner et al., 2021).

The EWSR1 gene, a member of the TET family (also known as FET) that is encoded on chromosome 22q12, was first noted to be rearranged in Ewing sarcoma (Aurias et al., 1983). The EWSR1 gene encodes an RNA/DNA binding protein and is ubiquitously

expressed in most cell types, indicating that it has multifunctional roles in diverse cellular processes (Lee et al., 2019). EWSR1 was shown to interact with the basal transcription factors Transcription factor II D and RNA Polymerase II (Bertolotti et al., 1998). In addition, EWSR1 was found to be associated with a transcriptional coactivator CREB-binding protein (Araya et al., 2003), suggesting that EWSR1 plays a central role in basic transcriptional regulation. However, the immunological function of EWSR1 is poorly defined owing to EWSR1 being identified in Ewing sarcoma cells, which are developmentally further from immune cells.

Here, by employing B cell–conditional *Ewsr1*-knockout mice, we found that EWSR1 functions as a brake to GC generation and IgG production under homeostatic conditions as well as to vaccination-induced GC formation and IgG responses. We further showed that a TNF receptor-associated factor (TRAF) family member, TRAF3, serves as a negative regulator of EWSR1. Under steady-state conditions, TRAF3 binds to EWSR1 and inhibits its nuclear translocation. Upon the signal-induced degradation of TRAF3, EWSR1 accumulates in the nucleus and modulates

¹Department of Cell Biology, School of Basic Medical Sciences, Nanjing Medical University, Nanjing, China; ²Houston Methodist Cancer Center, Houston Methodist Research Institute, Houston Methodist Hospital, Houston, TX, USA; ³Graduate Institute of Immunology, College of Medicine, National Taiwan University, Taipei, Taiwan; ⁴Department of Biological Sciences, Pusan National University, Busan, Korea; ⁵State Key Laboratory of Cellular Stress Biology, School of Life Sciences, Faculty of Medicine and Life Sciences, Xiamen University, Xiamen, China; ⁶Department of Bioinformatics and Computational Biology, The University of Texas MD Anderson Cancer Center, Houston, TX, USA; ⁷Memorial Hermann-Texas Medical Center, Houston, TX, USA; ⁸General Clinical Research Center, Nanjing First Hospital, Nanjing Medical University, Nanjing, China.

Correspondence to Zuliang Jie: jiezuliang@xmu.edu.cn; Shuli Zhao: shulizhao79@163.com; Yanchuan Li: liyanchuan2008@gmail.com.

© 2023 Li et al. This article is distributed under the terms of an Attribution–Noncommercial–Share Alike–No Mirror Sites license for the first six months after the publication date (see <http://www.rupress.org/terms/>). After six months it is available under a Creative Commons License (Attribution–Noncommercial–Share Alike 4.0 International license, as described at <https://creativecommons.org/licenses/by-nc-sa/4.0/>).



transcriptional regulation. These results establish the TRAF3–EWSR1 signaling axis acts as a checkpoint for GC response, revealing a new mechanism of GC formation.

Results

Unveil a novel TRAF3-mediated signaling pathway in GC responses

GCs formation requires the activation of the non-canonical NF- κ B family members p52 and RelB, as well as the upstream *Map3k14* gene encoding NIK (NF- κ B-inducing kinase) in B cells (Sun, 2017; Zhang et al., 2015). Loss of the negative regulator TRAF3 causes NIK accumulation, leading to constitutive p100 processing and p52/RelB nuclear translocation, which account for B cell accumulation and enlarged Peyer's patches (PPs; Liao et al., 2004; Sasaki et al., 2008; Xie et al., 2007). As expected, mice with B cell–conditional transgenic expression (*Mbl*-Cre allele) of *Map3k14* (*Map3k14^{Btg}*) or B cell–conditional deletion of *Traf3* (*Traf3^{BKO}*) had larger PP size and increased PP cell numbers as well as higher frequency and absolute number of B cells in PPs compared with those in WT control mice (Fig. 1, A, B, F, and G). Compared with the WT mice, the *Map3k14^{Btg}* mice also displayed a higher percentage and numbers of GC B cells and IgG1⁺ B cells in PPs (Fig. 1, C and D). Surprisingly, despite the uncontrolled non-canonical NF- κ B signaling, the *Traf3^{BKO}* mice did not display an abnormally high percentage of GC B cells and even had a lower percentage of IgG1⁺ B cells in PPs than that in WT mice (Fig. 1, H and I). Moreover, following immunization with a T cell–dependent antigen, 4-hydroxy-3-nitrophenylacetyl conjugated to keyhole limpet hemocyanin (NP-KLH), *Map3k14^{Btg}* mice showed higher NP-specific IgM and IgG responses compared with WT mice (Fig. 1 E). However, *Traf3^{BKO}* mice only showed an increased NP-specific IgM response and a normal NP-specific IgG response compared with those in WT mice (Fig. 1 J). These results suggest that TRAF3 must have another NIK-independent function involved in the regulation of GC B cell response that prevents the development of GC hyperplasia and IgG responses.

TRAF3 binds EWSR1 and inhibits its nuclear translocation

Previously, we employed proximity-dependent biotin identification (BioID) to screen for proteins interacting with TRAF3 (Li et al., 2021). One of the major TRAF3-binding proteins we identified was EWSR1. We confirmed the EWSR1/TRAF3 interaction by coimmunoprecipitation (coIP) assays and further revealed that this molecular interaction required the C-terminal TRAF domain (TRAF-C) of TRAF3 and the transcriptional activation domain of EWSR1 (Fig. 2, A–D). The interaction between TRAF3 and EWSR1 was also readily detected under endogenous conditions in B cells (Fig. 2 E). To determine the function of TRAF3 and EWSR1 interaction, we generated *Ewsr1* B cell–conditional knockout (*Ewsr1^{BKO}*) mice (Fig. S1 A). The EWSR1 deficiency did not affect the TRAF3 protein level or nuclear translocation or non-canonical NF- κ B activation (Fig. 2 F). Interestingly, TRAF3 deficiency in B cells increased the level of EWSR1, particularly the nuclear level of EWSR1, and this effect was not due to changes in *Ewsr1* mRNA expression (Fig. 2, G–I).

These results suggested that TRAF3 might regulate both the steady-state protein level and the nuclear translocation of EWSR1. To further ascertain the EWSR1-regulatory role of TRAF3, we determined whether signal-induced TRAF3 degradation could promote EWSR1 nuclear translocation. We stimulated B cells with B cell activating factor (BAFF), which is known to bind to BAFF receptor and stimulate TRAF3 degradation. Interestingly, BAFF-induced TRAF3 degradation in WT B cells was associated with the nuclear translocation of EWSR1. Furthermore, nuclear EWSR1 levels were high in TRAF3-deficient B cells without being affected by BAFF stimulation (Fig. 2 J). These results, along with the EWSR1–TRAF3 interaction, suggest that TRAF3 functions as a negative regulator of EWSR1 that controls the nuclear translocation, and possibly stability of EWSR1.

EWSR1 controls the commitment of activated B cells to GC reaction and humoral immunity

We performed a detailed study of the in vivo function of EWSR1 in B cells by generating *Ewsr1^{BKO}* mice (Fig. S1). The *Ewsr1^{BKO}* mice were born at the expected Mendelian ratios and were grossly normal in growth and survival (data not shown). They also demonstrated intact B cell development, as suggested by the presence of similar B cell subpopulations in the bone marrow (Fig. S2, A and B) and spleen (Fig. S2, C–F) of *Ewsr1^{BKO}* and WT mice. In addition, *Ewsr1^{BKO}* and WT mice exhibited similar PP sizes and numbers as well as similar PP B cell percentages and absolute cell numbers (Fig. 3 A and Fig. S2 C). Strikingly, *Ewsr1^{BKO}* mice had a twofold higher frequency and number of PP GC B cells than WT mice under homeostatic conditions (Fig. 3 B).

To further investigate the possibility of a selective increase of a particular GC B cell subpopulation, we determined the fractions of the dark zone (DZ) and light zone (LZ) GC B cells based on the markers CXCR4 and CD86. However, there were no statistically significant differences in the DZ/LZ ratio between *Ewsr1^{BKO}* and WT control mice (Fig. 3 C). Follicular dendritic cells are known to present antigens to GC B cells in the form of immune complexes and are crucial for the formation and maintenance of GCs (El Shikh et al., 2010). Herein, we found that the deficiency of EWSR1 in B cells did not affect the follicular dendritic cell population in PPs (Fig. 3 D). PPs are a dominant site for the activation of IgA⁺ B cells (Round and Mazmanian, 2009). Interestingly, *Ewsr1^{BKO}* mice and WT mice had comparable IgA⁺ B cells in PP, but *Ewsr1^{BKO}* mice had a substantially higher percentage and absolute cell number of IgG1⁺ B cells (Fig. 3 E). Moreover, compared with WT control mice, the *Ewsr1^{BKO}* mice had significantly higher concentrations of serum antibodies, including IgG, IgG1, IgG2b, and IgG2c, as well as elevated concentrations of fecal IgG (Fig. 4, A and B). Together, these results demonstrated that EWSR1 has a central role in controlling GC formation and IgG production under steady-state conditions, which is most likely due to mucosal lymphoid tissue that encounters foreign antigens from the intestine.

To determine whether EWSR1 also regulates GC formation induced by immunization, we challenged the *Ewsr1^{BKO}* and WT control mice with a T cell–dependent antigen, NP-KLH. Compared with the WT mice, the *Ewsr1^{BKO}* mice displayed a significantly higher serum concentration of NP-specific IgG and IgG1

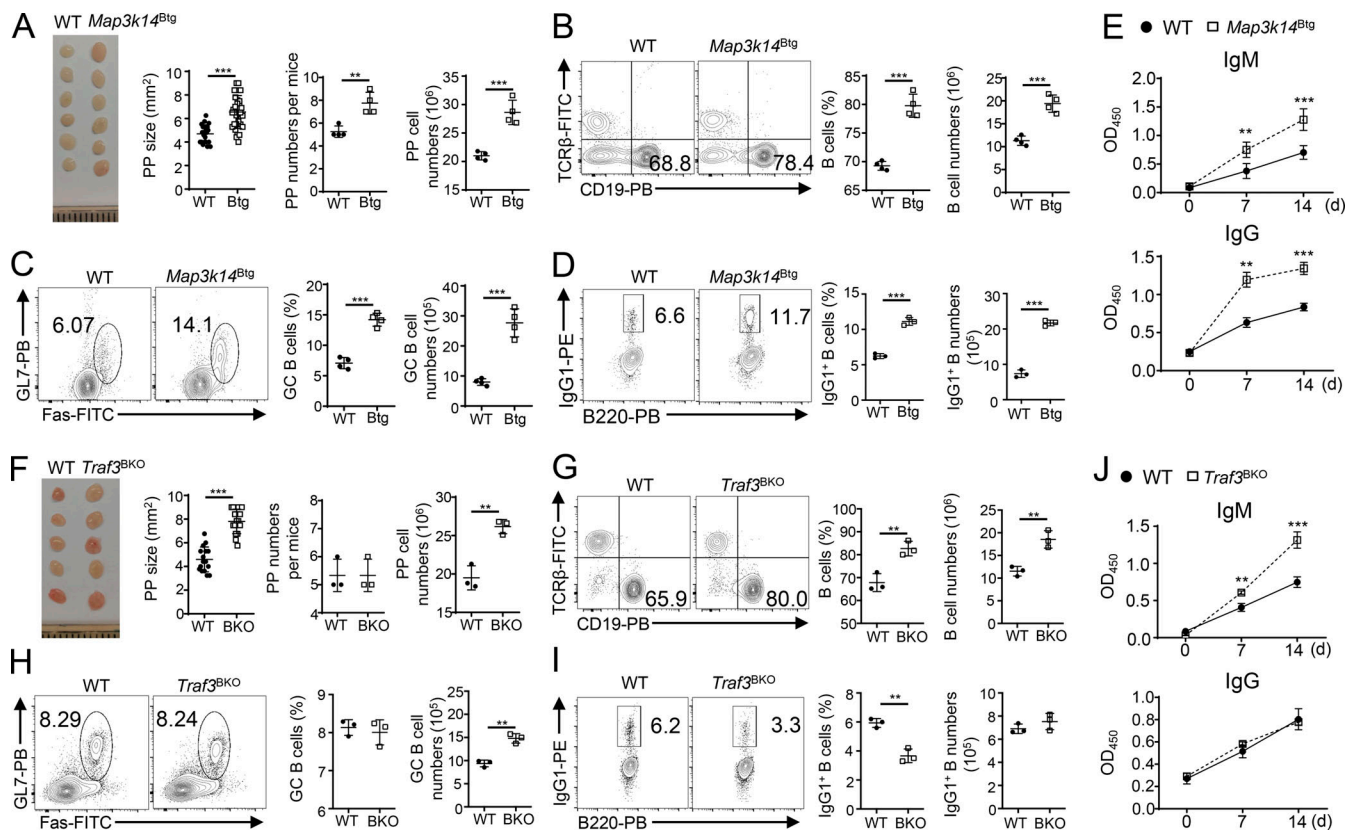


Figure 1. Analysis of GC homeostasis and humoral immunity in *Map3k14^{Btg}* and *Traf3^{BKO}* mice. (A) Representative PP image and summary graphs of PPs size (WT: *n* = 21, Btg: *n* = 31), numbers and cell numbers of WT and *Map3k14^{Btg}* mice (*n* = 4 mice/group, 6–8 wk old). (B) Flow cytometric analysis of CD19⁺ B cells in PPs of WT or *Map3k14^{Btg}* mice (*n* = 4 mice/group, 6–8 wk old). (C) Flow cytometric analysis of GC B cells (B220⁺ GL7⁺ Fas⁺) in PPs of WT or *Map3k14^{Btg}* mice (*n* = 4 mice/group, 6–8 wk old). (D) Flow cytometric analysis of IgG1⁺ B cells in PPs of WT or *Map3k14^{Btg}* mice (*n* = 4 mice/group, 6–8 wk old). (E) T cell–dependent immune response in WT and *Map3k14^{Btg}* mice (*n* = 5 mice/group, 6–8 wk old). Serum levels of NP-specific IgM and IgG were measured by ELISA at indicated time points. (F) Representative PPs image and summary graphs of PP size (WT: *n* = 16, BKO: *n* = 16), and cell numbers of WT and *Traf3^{BKO}* mice (*n* = 3 mice/group, 6–8 wk old). (G) Flow cytometric analysis of CD19⁺ B cells in PPs of WT or *Traf3^{BKO}* mice (*n* = 3 mice/group, 6–8 wk old). (H) Flow cytometric analysis of GC B cells in PPs of WT or *Traf3^{BKO}* mice (*n* = 3 mice/group, 6–8 wk old). (I) Flow cytometric analysis of IgG1⁺ B cells in PPs of WT or *Traf3^{BKO}* mice (*n* = 3 mice/group, 6–8 wk old). (J) T cell–dependent immune response in WT and *Traf3^{BKO}* mice (*n* = 5 mice/group, 6–8 wk old). Serum levels of NP-specific IgM and IgG were measured by ELISA at indicated time points. Data are representative of three independent experiments. Summary graphs are presented as mean ± SD (A–D and F–I) or mean ± SEM. (E and J) P values were determined by unpaired two-tailed Student’s *t* test. ***P* < 0.01 and ****P* < 0.001.

(Fig. 4 C). In contrast, the *Ewsr1^{BKO}* and WT mice did not display significant differences in IgG concentration when immunized with a T cell-independent antigen, NP-Ficoll (Fig. 4 D), indicating that EWSR1 is selectively required for regulating T cell-dependent antibody responses.

The increased number of GCs may result from an increase in either division of GC B cells or the inflow of activated B cells into the GC response. To test these possibilities, we analyzed the proliferating or apoptotic PP GC B cells that were freshly isolated from *Ewsr1^{BKO}* and WT control mice. These results indicated that the increased number of GCs in *Ewsr1^{BKO}* mice was not associated with differences in proliferating or dying B cells within the GC (Fig. 4, E and F). We evaluated GC percentages, size, and numbers after performing NP-KLH immunization by flow cytometry and immunohistochemistry analysis, respectively. Notably, *Ewsr1^{BKO}* mice displayed higher percentages and numbers of GCs than WT mice upon immunization (Fig. 4, G and H). However, GC size did not significantly change in *Ewsr1^{BKO}* mice

when compared with control mice (Fig. 4 H). Together, these data suggest that loss of EWSR1 lowers the threshold at which activated B cells enter the GC reaction but does not cause enhancement of cell division by GC B cells.

NIK-independent function of TRAF3 in regulation GC B cell response relies on EWSR1

To determine how the accumulation of nuclear EWSR1 in TRAF3-deficient B cells contributes to the differences in GC B cell response between *Map3k14^{Btg}* mice and *Traf3^{BKO}* mice, we generated mutant mice carrying B cell-specific deficiencies in both TRAF3 and EWSR1. Regardless of whether EWSR1 was deleted, TRAF3 deficiency in B cells caused significantly higher amount of B cells in the spleen, inguinal lymph nodes, and PPs (Fig. 5 A). Moreover, consistent with prior studies, *Traf3^{BKO}* mice had normal GC B cell percentages and even lower IgG1⁺ B cell percentages in PPs (Fig. 5 B). Interestingly, EWSR1 deletion in *Traf3^{BKO}* mice greatly enhanced the frequency of GC B cells

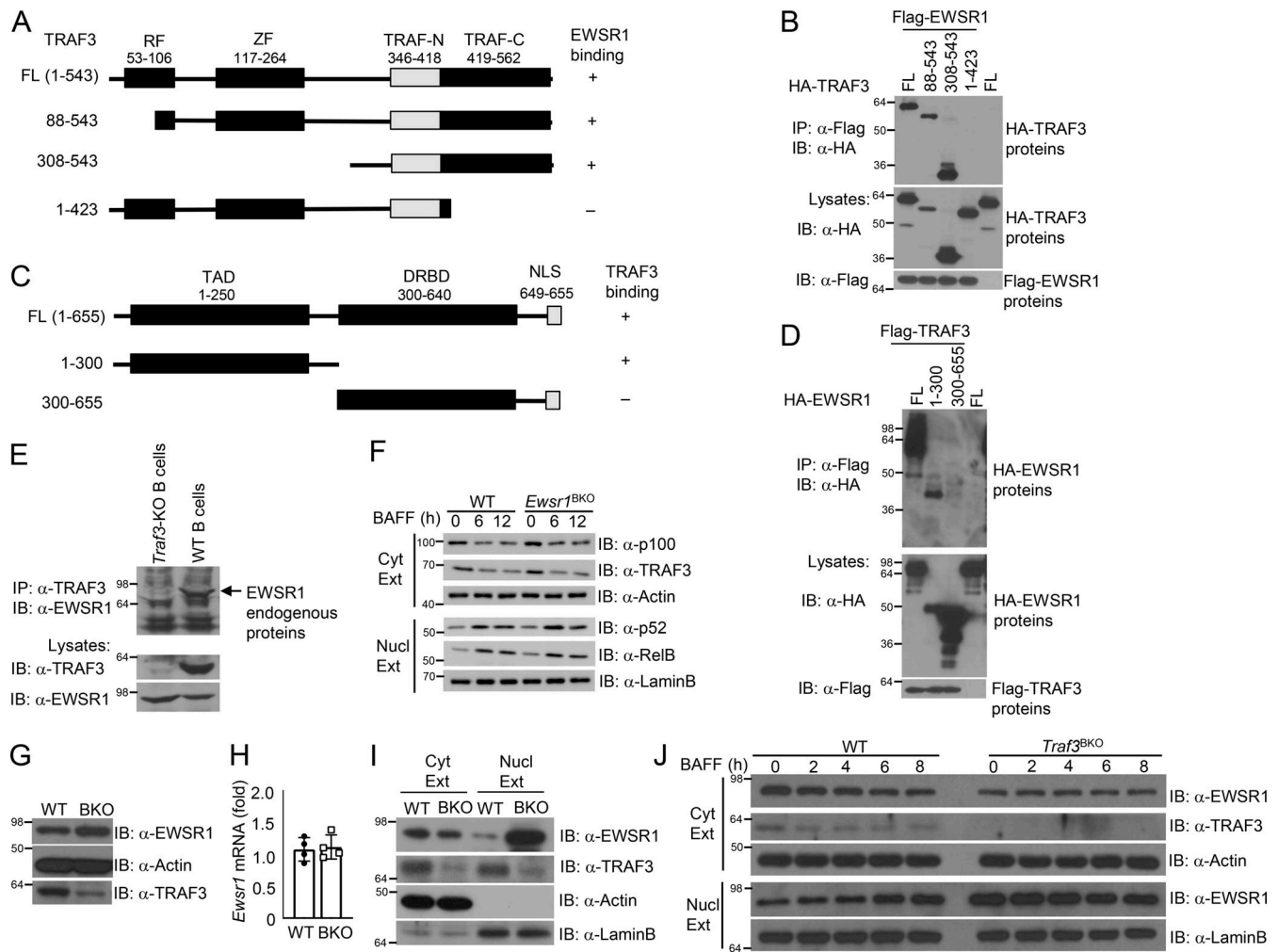


Figure 2. TRAF3 regulates EWSR1 nuclear localization via protein interaction. (A) Schematic diagram of TRAF3 and its truncation mutants, depicting the ring finger (RF), zinc finger (ZF), and TRAF (TRAF-N and TRAF-C) domains and indicating their EWSR1-binding affinity based on the colP results from B. (B) ColP analysis of EWSR1 interaction with TRAF3 mutants using whole-cell lysates of HEK293 cells transfected with the indicated expression vectors. Cell lysates were also subjected to direct immunoblotting (IB) to monitor the expression of TRAF3 mutants and EWSR1. (C) Schematic diagram depicting the transcriptional activation domain (TAD), DNA- and RNA-binding domains (DRBD), and nuclear localization signals (NLS) of EWSR1 and its mutants and their ability to bind TRAF3 (based on colP results of D). (D) ColP analysis of TRAF3 interaction with EWSR1 mutants using whole-cell lysates of HEK293 cells transfected with the indicated expression vectors (upper). Cell lysates were also subjected to direct immunoblotting to monitor the expression of EWSR1 mutants and TRAF3 (lower). (E) ColP analysis of endogenous TRAF3/EWSR1 interaction in splenic B cells. TRAF3 deleted B cells were used as a negative control. (F) Immunoblot analysis of the indicated proteins using cytoplasmic or nuclear extracts of WT and *Ewsr1*^{BKO} splenic B cells stimulated as indicated. (G) Immunoblot analysis of the indicated proteins in whole-cell lysates of freshly isolated splenic B cells from WT and *Traf3*^{BKO} mice. (H) RT-qPCR analysis of *Ewsr1* mRNA in WT and *Traf3*^{BKO} splenic B cells. (I) Immunoblot analysis of the indicated proteins using cytoplasmic (Cyt Ext) and nuclear (Nucl Ext) extracts of freshly isolated splenic B cells from WT and *Traf3*^{BKO} mice. (J) Immunoblot analysis of the indicated proteins using cytoplasmic or nuclear extracts of WT and *Traf3*^{BKO} splenic B cells stimulated as indicated. Data are representative of three independent experiments. The molecular weight measurements are kD. Source data are available for this figure: SourceData F2.

and IgG1⁺ B cells in PPs (Fig. 5 B). These results indicate that EWSR1 deletion could largely rescue the differences in GC B cell response between *Map3k14*^{Btg} mice and *Traf3*^{BKO} mice, despite the unaffected non-canonical NF-κB signaling.

EWSR1-mediated GCs regulation involves modulation of Bcl6 expression in antigen-activated B cells

To assess the mechanism by which EWSR1 regulates GC responses, we examined the effect of EWSR1 deficiency on GC B cell gene expression profile under homeostatic conditions in vivo. We analyzed the gene expression profile of WT and

EWSR1-deficient PP GC B cells by RNA sequencing (RNA-seq). This experiment, which was based on the results of three independent samples, revealed significant alterations in the expression of two genes with particular interest: Bcl6, a master regulator of the GC reaction (Basso and Dalla-Favera, 2010), and Cd55, an inhibitor of complement signaling (Lublin and Atkinson, 1989; Table S2). To gain a deeper understanding of EWSR1 deficiency on GC B cell gene expression profile that influences the differentiation of B cells, we performed gene set enrichment analysis (GSEA) in the global gene expression profiles of naive B cells with those of antigen-specific GC B cells after immunization

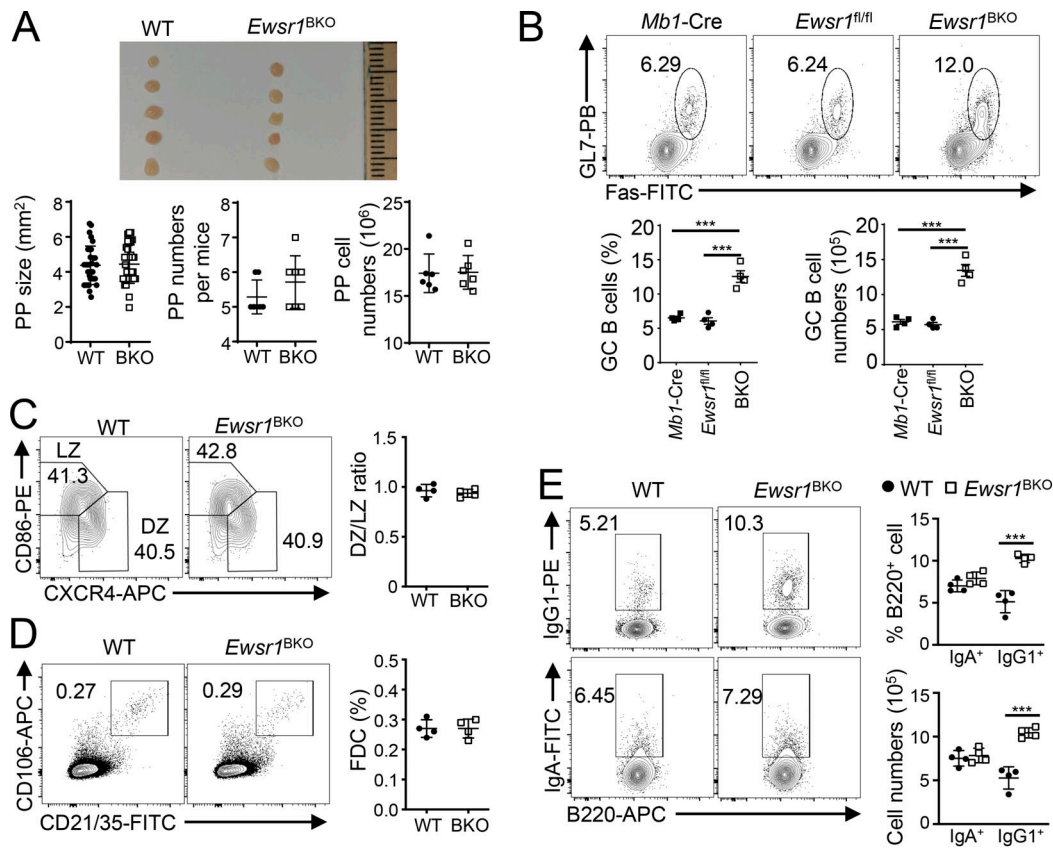


Figure 3. *Ewsr1* controls GC generation in PPs under homeostatic conditions. (A) Representative image and summary graphs of PP size (WT: $n = 32$, BKO: $n = 32$), numbers, and cell numbers in WT and *Ewsr1*^{BKO} mice ($n = 6$ mice/group, 6–8 wk old). (B) Flow cytometric analysis of GC B cells in PPs of WT (*Mb1-Cre* and *Ewsr1*^{fl/fl}) or *Ewsr1*^{BKO} mice ($n = 4$ mice/group, 6–8 wk old). (C) Flow cytometric analysis of the DZ (CXCR4^{high}CD86^{low}) and LZ (CXCR4^{low}CD86^{high}) ratio in the PPs of WT and *Ewsr1*^{BKO} mice ($n = 4$ mice/group, 6–8 wk old). (D) Flow cytometric analysis of follicular dendritic cells (FDC; CD45⁺CD31⁺CD106⁺CD21/35⁺) in PPs of WT or *Ewsr1*^{BKO} mice ($n = 4$ mice/group, 6–8 wk old). (E) Flow cytometric analysis of IgG1⁺ B cells and IgA⁺ B cells in PPs of WT or *Ewsr1*^{BKO} mice ($n = 4$ mice/group, 6–8 wk old). Data are representative of three independent experiments. Summary graphs are presented as mean \pm SD. P values were determined by an unpaired two-tailed Student's *t* test. ****P* < 0.001.

with the T dependent antigen. Although the naive and GC B cells share a large portion of their transcriptional profiles, these genes, which were downregulated in the *Ewsr1*-deficient B cells, were enriched in the bulk expression profile of GC B cells compared with naive B cells (Fig. 6 A). This further supports the idea that EWSR1 plays a role in regulating GC B cell commitment. Flow cytometric analyses confirmed the significant downregulation of CD55 and upregulation of BCL6 in EWSR1-deleted B cells (Fig. S3 A and Fig. 6 B). Of note, CD55 has been shown to inhibit complement activation by acting on the complement C3 convertases and thereby regulates B cell activation, antigen uptake, processing, and presentation (Cherukuri et al., 2001; Lublin and Atkinson, 1989; Nielsen et al., 2000). We determined whether the increased GC responses in *Ewsr1*^{BKO} mice were a result of enhanced complement activation. To test this possibility, we crossed the *Ewsr1*^{BKO} mice with mice that were deficient in a major complement component, C3 (C3 KO). This C3 deficiency did not reduce the frequency of GC B cells and only moderately reduced the frequency of IgG1⁺ B cells in the PPs under homeostatic conditions (Fig. S3 B). Furthermore, C3 deletion in *Ewsr1*^{BKO} mice did not prevent abnormally high levels of PP GC B cells and IgG1⁺ B cells (Fig. S3 B). These data suggest that

the complement system is not involved in the homeostatic GC regulation by the TRAF3–EWSR1 signaling axis.

In a further effort to predict the mechanism of EWSR1 function, we screened EWSR1 chromatin immunoprecipitation sequencing (ChIP-seq) results using GSM2472081 and GSM2472082 datasets from the GEO database with the accession number GSE94275 (Boulay et al., 2017). Interestingly, these analyses revealed that EWSR1 binding is enriched at the first intron of *Bcl6* (Fig. 6 C), which is known as a negatively regulated region of this pivotal GC-associated gene (Kikuchi et al., 2000). This finding was in line with our observation that *Bcl6* gene expression was upregulated in the *Ewsr1*^{BKO} mouse B cells (Fig. 6 B and Table S2). To validate ChIP-seq results, we designed two primer pairs within the first intron of *Bcl6* and performed ChIP quantitative PCR (qPCR) in BJAB cell line which overexpressed HA-EWSR1 (Fig. 6 D). In addition to its function as a transcription factor, EWSR1 is known to serve as an RNA-binding protein (Tan and Manley, 2009). We thus also performed RNA pull-down assay to test the possibility of RNA regulation of *Bcl6* (Fig. 6 E). These results suggest that EWSR1 regulates BCL6 via direct DNA binding but not RNA–protein interactions. By modulating the amount of *Bcl6* expression in transgenic mice,

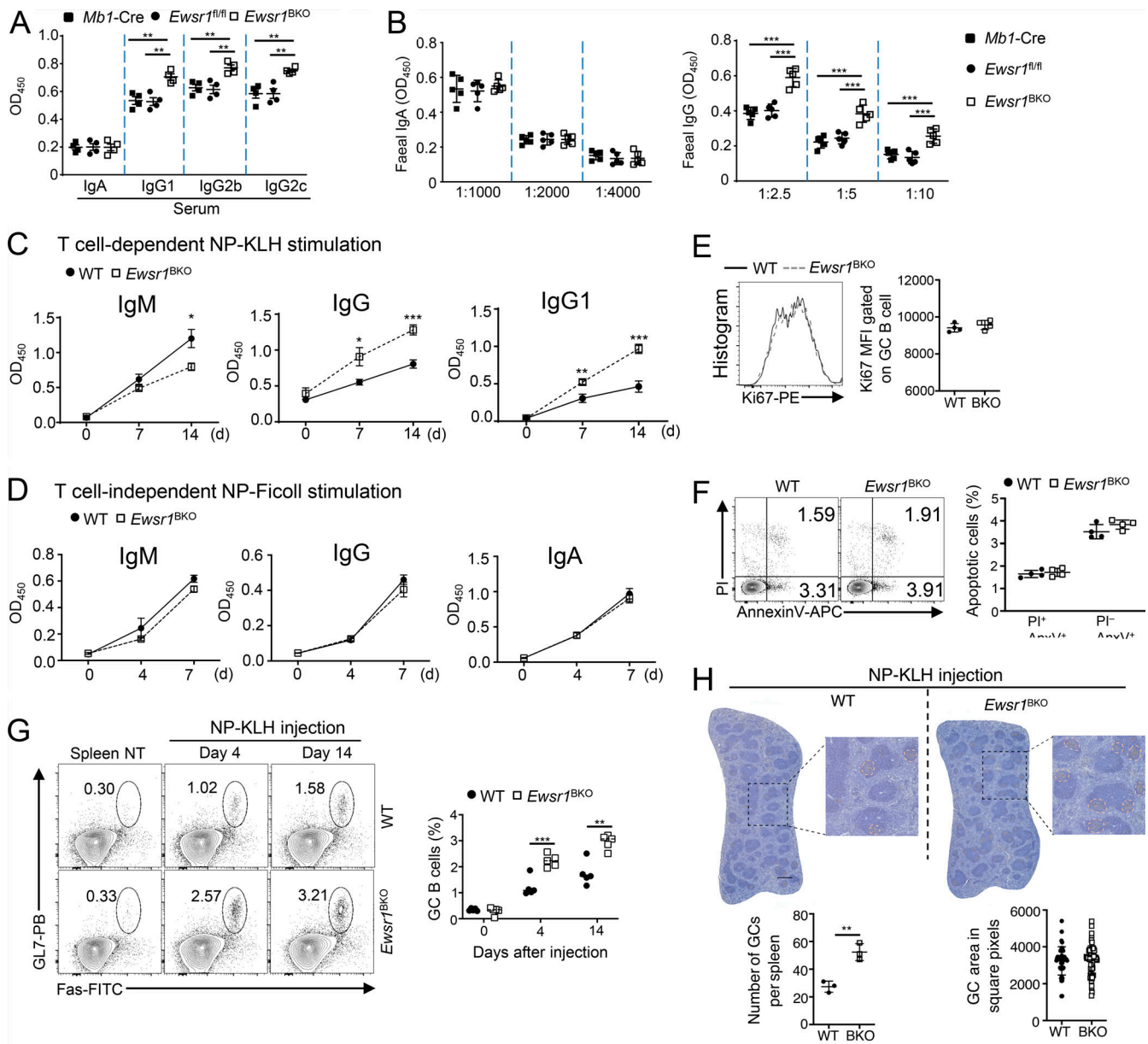


Figure 4. Increased IgG antibody responses in *Ewsr1^{BKO}* mice. (A and B) ELISA analysis of basal IgG isotype levels in serum (A; $n = 4$ mice/group, 8 wk old) or fecal (B; $n = 5$ mice/group, 8 wk old) samples from non-immunized WT (*Mb1-Cre* and *Ewsr1^{fl/fl}*) and *Ewsr1^{BKO}* mice. **(C)** ELISA analysis kinetics of NP-specific IgM, IgG, and IgG1 production after NP-KLH-immunized WT and *Ewsr1^{BKO}* mice ($n = 8$ mice/group, 6–8 wk old). **(D)** ELISA analysis kinetics of NP-specific IgM, IgG, and IgG1 production after NP-Ficoll-immunized WT and *Ewsr1^{BKO}* mice (WT: $n = 6$, BKO: $n = 6$, 6–8 wk old). **(E)** Flow cytometric analysis of proliferating cells (Ki67⁺) in the PPs of WT and *Ewsr1^{BKO}* mice GC B cells ($n = 4$ mice/group, 6–8 wk old). **(F)** Flow cytometric analysis of apoptotic cells based on Annexin V and propidium iodide (PI) staining in the PPs of WT and *Ewsr1^{BKO}* mouse GC B cells ($n = 4$ mice/group, 6–8 wk old). **(G)** Flow cytometric analysis of the frequency of GC B cells in WT and *Ewsr1^{BKO}* mice immunized with NP-KLH for the indicated days ($n = 5$ mice/group, 6–8 wk old). **(H)** Immunohistochemical staining of GCs (peanut agglutinin⁺) in splenic sections from G on day 14. Scale bar: 500 μ m. GC area was quantified by ImageJ. Data are representative of two (G and H) or at least three (A–F) independent experiments. Summary graphs are presented as mean \pm SD. P values were determined by an unpaired two-tailed Student's *t* test. * $P < 0.05$; ** $P < 0.01$; *** $P < 0.001$.

a recent study demonstrates that Bcl6^{hi} B cells responding to immunization are more likely to commit to the GC program (Robinson et al., 2020). In line with this recent work, our data suggested that EWSR1 might regulate GC B cell transition rather than GC B cell maintenance, further implying a role of EWSR1 in Bcl6 regulation. The low amount of BCL6 induced during the early phase of B cell activation is central to determining GC commitment and thus memory B cell populations, whereas

such a low level of BCL6 does not affect other BCL6-regulated GC B cell behaviors (Robinson et al., 2020). We found that EWSR1 deletion resulted in a moderate upregulation of BCL6 level, with about a 30% increase (Fig. 6 B and Table S2). Furthermore, Bcl6 was upregulated in EWSR1-deficient PP B cells, including both GC B cells and pre-GC B cells (Fig. 6 B). In contrast, B cells from non-foreign antigen-exposed tissue, such as inguinal lymph nodes and spleen Bcl6-expressing, were

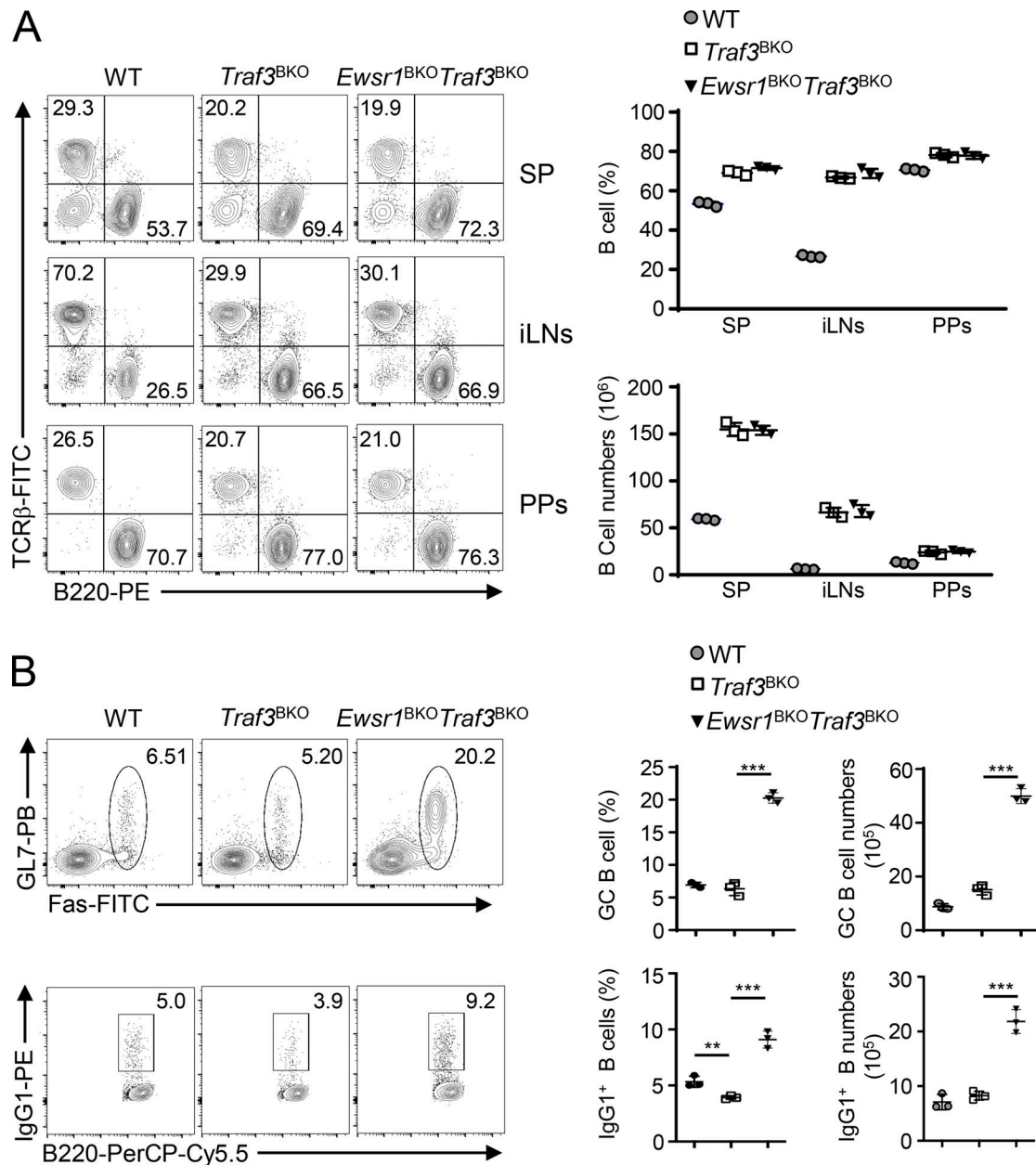


Figure 5. **Flow cytometric analysis of B cell and GC homeostasis in WT, *Traf3*^{BKO}, and *Traf3*^{BKO}*Ewsr1*^{BKO} mice.** (A) Flow cytometric analysis of B220⁺ B cells and TCRβ⁺ T cells in the spleen (SP), inguinal lymph nodes (iLNs), and PPs of WT, *Traf3*^{BKO}, and *Traf3*^{BKO}*Ewsr1*^{BKO} mice (*n* = 3 mice/group, 6–8 wk old). (B) Flow cytometric analysis of GC B cells and IgG1⁺ B cells in PPs of WT, *Traf3*^{BKO}, and *Traf3*^{BKO}*Ewsr1*^{BKO} mice (*n* = 3 mice/group, 6–8 wk old). Data are representative of two independent experiments. Summary graphs are presented as mean ± SD, and P values were determined by unpaired two-tailed Student's *t* test. ***P* < 0.01 and ****P* < 0.001.

comparable between WT and *Ewsr1*^{BKO} mice (Fig. 6 B), suggesting that the TRAF3–EWSR1 axis regulates Bcl6 expression specifically in foreign antigen–engaged B cells.

We performed a single-cell RNA-seq (scRNA-seq) analysis of PP B cells using graph-based clustering to partition PP B cells into seven clusters (Fig. S4 A) that were identified through the marker gene list in Fig. S4 C. The results indicated the presence of a reduced fraction of follicular/marginal zone B cells and increased pre-GC and activated GC B cells, as well as post-GC memory B cells, which further establishes that EWSR1 deficiency increases GC B cell transition (Fig. 6 F). Interestingly, the

Ewsr1 expression level in WT mice was also significantly higher in pre-GC B cells, activated GCs, and memory B cells, emphasizing the role of EWSR1 in these clusters (Fig. S4 B). Moreover, flow cytometric analysis confirmed that *Ewsr1*^{BKO} mice had an increased frequency and number of pre-GC B cells (CD38^{hi}GL7⁺) and CD38^{int}GL7⁺ B cells in PPs compared with those in WT mice (Fig. 6 G). Reciprocally, the results of previous studies suggested that antigen-engaged B cells upregulated Bcl6 in pre-GC B cells (Kerfoot et al., 2011; Kitano et al., 2011), indicating that *Ewsr1* regulates Bcl6 mainly starting at pre-GC B cells entry to GC clusters.

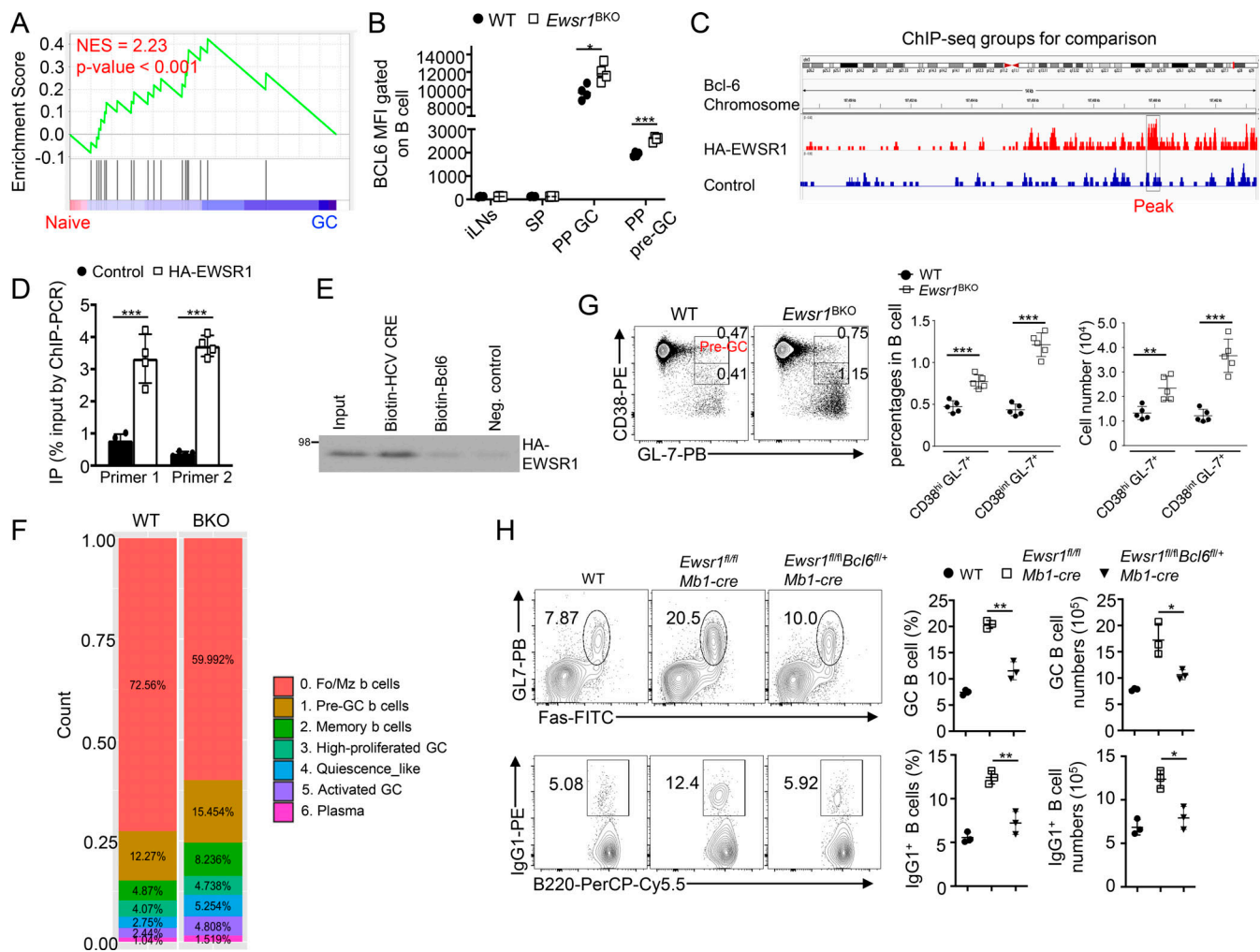


Figure 6. Bcl6 contributes to EWSR1-mediated GC regulation. (A) GSEA analysis of differentially expressed genes between WT and *Ewsr1*-deficient B cells (listed in Table S2) based on the expression profiles of purified bulk populations from naive B cells versus GC B cells after immunization with the T dependent antigen. NES, normalized enrichment score. (B) Flow cytometric analysis of Bcl6 expression using median fluorescence intensity (MFI) on gated B cells as indicated ($n = 4$ mice/group, 6–8 wk old). (C) Genomic location annotation and ChIP-seq peaks analysis of HA-EWSR1 and control DNA-binding specificity in A549 cells. (D) ChIP-PCR detecting the binding of EWSR1 to the first intron region of the Bcl6 gene using two different primers in BJAB cells transfected with HA-EWSR1 or control plasmid. (E) Analysis of the binding of HA-EWSR1 with Biotin-labeled Bcl6 by RNA pull-down assay. Biotin-labeled HCV CRE was the positive control. The molecular weight measurements are kD. (F) Frequency plot of each B cell population between WT and *Ewsr1*^{BKO} mice according to Seurat cluster identification. Fol/MZ, follicular/marginal zone. (G) Flow cytometric analysis of pre-GC B cells (B220⁺ CD38^{int}GL7⁺) and CD38^{int}GL7⁺ B cells in PPs of WT or *Ewsr1*^{BKO} mice ($n = 4$ mice/group, 6–8 wk old). (H) Flow cytometric analysis of GC B cells and IgG1⁺ B cells in PPs of WT, *Ewsr1*^{fl/fl}Mb1-Cre, and *Ewsr1*^{fl/fl}Bcl6^{fl/fl}Mb1-Cre mice ($n = 3$ mice/group, 6–8 wk old). Data are representative of one (A and F) or two (B, D, E, G, and H) independent experiments. Summary graphs are presented as means \pm SD, and P values were determined by an unpaired two-tailed Student's t test. * $P < 0.05$; ** $P < 0.01$; and *** $P < 0.001$. Source data are available for this figure: SourceData F6.

To determine the functional contribution of BCL6 to GC formation and IgG response in *Ewsr1*^{BKO} mice, we crossed *Ewsr1*^{BKO} mice with *Bcl6*^{fl/fl} mice. Since Bcl6 KO mice display severe defects in GC B cells (Dent et al., 1997), we examined heterozygous *Ewsr1*^{fl/fl}*Bcl6*^{fl/fl}Mb1-Cre mice. Remarkably, the heterozygous null Bcl6 allele in *Ewsr1*^{BKO} mice exhibited a profoundly reduced frequency and the absolute number of PP GC B cells and IgG1⁺ B cells and largely erased the differences between *Ewsr1*^{BKO} and WT mice (Fig. 6 H). Overall, these results suggest that EWSR1-mediated GC regulation involves the modulation of Bcl6 expression.

TRAF3-EWSR1 axis blockade in B cells control *Citrobacter rodentium* infection

Under homeostatic conditions, the gut microbiota induces the production of IgG, which mainly recognizes gram-negative commensal antigens and confers protection against systemic infection (Zeng et al., 2016). Given the critical role of EWSR1 in regulating PP GC B cell generation and IgG production under steady-state conditions, we investigated the role of EWSR1 in regulating microbiota composition and pathogen infections. To examine the effect of EWSR1 deficiency on microbiota composition, we performed 16S ribosomal RNA-seq analysis using fecal

RNA from *Ewsr1*^{BKO} and WT mice housed under specific pathogen-free conditions. Principal coordinate analysis did not reveal significant differences in microbial communities between *Ewsr1*^{BKO} and WT control mice (Fig. S5). These results suggest that EWSR1 deletion in B cells had no obvious effect on the microbiota composition under homeostatic conditions, which is in line with a study suggesting that IgG recognizes virulent pathogens but not commensals or avirulent pathogens (Kamada et al., 2015). Next, we examined the role of EWSR1 in regulating mucosal immunity against infections using a well-characterized mouse intestinal gram-negative virulent pathogen, *C. rodentium*. Compared with WT mice, the *Ewsr1*^{BKO} mice displayed much milder pathogenic symptoms, including colonic shortening (Fig. 7, A and B), as well as colonic crypt hyperplasia and inflammatory cell infiltration (Fig. 7 D). Consistently, the *Ewsr1*^{BKO} mice were considerably more resistant to *C. rodentium* infection, as shown by the significantly reduced bacterial load in organs and feces (Fig. 7, C and F). The *Ewsr1*^{BKO} mice also had less severe body weight loss (Fig. 7 E), coupled with an increased concentration of *C. rodentium*-specific sera IgG (Fig. 7 G). Interestingly, compared with the symptom relief, induction of *C. rodentium*-specific IgG was delayed. This result indicates that the constitutively elevated IgG under steady-state conditions provides early protection in *Ewsr1*^{BKO} mice, which is consistent with homeostatic IgG being important for protection against infectious challenges in the intestine (Caballero-Flores et al., 2019; Maaser et al., 2004; Masuda et al., 2008; Zeng et al., 2016).

Since an increase in IgG production was a major immunological phenotype of *Ewsr1*^{BKO} mice, we evaluated the contribution of IgG antibodies to defense against *C. rodentium* infection in *Ewsr1*^{BKO} mice. We performed the passive immunization experiments by injecting sera collected from WT or *Ewsr1*^{BKO} mice, which had been infected by *C. rodentium* 3 wk before, into *C. rodentium*-infected WT mice (Fig. 7 H). Compared with the sera from WT mice, the sera from *Ewsr1*^{BKO} mice were more protective, as revealed by milder body weight loss and significantly decreased fecal bacterial load (Fig. 7, I and J). Importantly, such a protective function was dependent on IgG since depletion of IgG abolished the *C. rodentium*-protective function of the sera and erased the protective differences between the *Ewsr1*^{BKO} and WT mouse sera (Fig. 7, I and J). Collectively, these findings suggest that increased IgG production in *Ewsr1*^{BKO} mice contributes to their stronger immunity against *C. rodentium* infection. These data also imply that targeting the TRAF3-EWSR1 signaling axis may be an approach to enhance humoral immunity against infections.

Discussion

In this study, we have identified that the TRAF3-EWSR1 signaling axis acts as a checkpoint on GC responses. B cell-specific deletion of *Ewsr1* profoundly enhances GC responses and IgG production under homeostatic conditions as well as vaccination-induced GCs formation and IgG responses, suggesting that inhibition of this pathway could unleash GC responses leading to profoundly stronger immunity against infections. Mechanistically, TRAF3 binds to EWSR1 and inhibits the nuclear translocation of EWSR1, thereby preventing its action to suppress GC

responses. Upon signal-induced degradation of TRAF3, EWSR1 accumulates in the nucleus and suppresses the expression of Bcl6, a master transcription factor mediating GC B cell generation and IgG production. Interestingly, we also found that several genes that are known to be directly suppressed by BCL6 were downregulated in the EWSR1-deficient GC B cells (Cumpelik et al., 2021; Yoshida et al., 2011; Young and Brink, 2021), including *Ccr6*, *S1pr1*, *Cd55*, *Cd63*, etc. This implies that these genes are indirectly regulated by BCL6.

The initiation of the GC reaction involves activation of the B cell receptor by antigen encounter and requires an interaction between B cells and antigen-presenting cells and helper T cells (Cyster and Allen, 2019; Victora and Nussenzweig, 2022). It is now clear that several signaling pathways are necessary to mediate the initiation of the GC reaction, which triggers TRAF3 degradation. One prominent signaling pathway is CD40 signaling, as the injection of antibodies that block the CD40-CD40L interaction leads to the acute dissolution of the GC reaction (Han et al., 1995). Additionally, BAFF signaling also plays a critical role in both GC formation and maintenance (Scholz et al., 2008). These signals eventually allow B cells to upregulate Bcl6, which is essential for GC formation (Fukuda et al., 1997), although detailed mechanisms of inducing the expression of BCL6 following antigenic stimulation remain elusive. BCL6 functions mainly as a transcriptional repressor that controls B cell positioning by negatively regulating the expression of cell migration receptors, such as *S1PR1* and *GPR183* (Suan et al., 2017). BCL6 also represses the anti-apoptotic molecule Bcl2 in GC B cells, ensuring the maintenance of a proapoptotic state, which is critical for affinity-based selection and prevention of autoimmunity (Saito et al., 2009). Thus, by direct and indirect mechanisms, BCL6 orchestrates the expression of a large network of genes controlling diverse cellular processes that are important to generate and/or sustain GC B cell phenotype.

The primary function of GCs is to generate high-affinity antibodies against foreign antigens that form a key defense against infectious pathogens and are crucial to the efficacy of almost all vaccines. On the other hand, GCs reported to be numerous in autoimmune-prone murine strains and known to arise spontaneously without immunization or infection are regarded as spontaneous GCs (Arkatkar et al., 2017; Beccaria et al., 2018; Domeier et al., 2016). Intriguingly, several studies have identified signaling pathways or factors that are essential for spontaneous GC responses but are not required for the GC responses induced by foreign antigens, suggesting that different mechanisms may control autoimmune spontaneous GC and induce GC responses (Domeier et al., 2017). However, the distinct mechanisms that control autoimmune spontaneous GC and induce GC responses remain elusive. Identifying the TRAF3-EWSR1 signaling axis as a key “brake” of induced GC responses provides insight into the mechanism that controls this important process and further application of this knowledge against infectious diseases, limiting the risks of non-specific autoimmune disease. Of note, under steady-state conditions, the TRAF3-EWSR1 signaling axis seems to regulate GC responses, specifically in PPs, a mucosal lymphoid tissue that encounters foreign

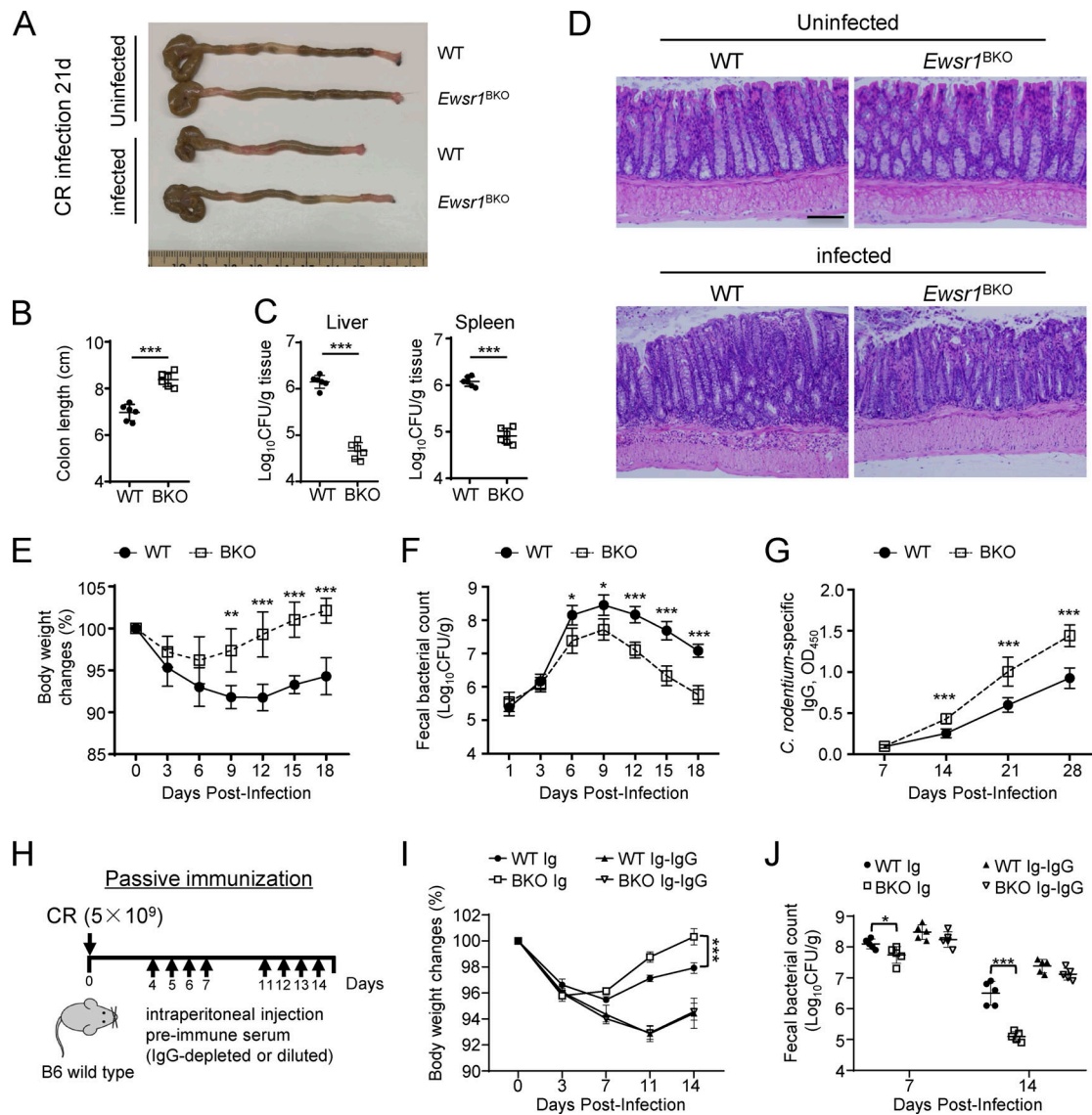


Figure 7. EWSR1 negatively regulates host defense against *C. rodentium* infection. WT and *Ewsr1*^{BKO} mice ($n = 6$ mice/group, 6–8 wk old) were orally infected with 5×10^9 CFU of *C. rodentium*. The infected and control mice were sacrificed 21 d after infection. **(A–G)** The colon length (A and B), bacteria titers in the liver and spleen (C), and colon histological staining with H&E with a scale bar of 200 μ m (D) were analyzed. Bodyweight changes (E), fecal *C. rodentium* titers (F), and *C. rodentium*-specific IgG production in serum (G) were examined at indicated timepoints. We performed the passive immunization experiments by injecting preimmune sera into *C. rodentium*-infected mice. To generate immune serum, WT or *Ewsr1*^{BKO} mice were infected with *C. rodentium* and sera were collected 3 wk later. IgG-depleted or non-depleted immune sera were injected into *C. rodentium*-infected mice. **(H)** Schematic of experimental design for passive immunization. **(I and J)** Bodyweight changes (I) and fecal *C. rodentium* titers (J) were detected in the feces of *C. rodentium*-infected mice as indicated ($n = 5$ mice/group, 6–8 wk old). Data are representative of two independent experiments. Summary graphs are presented as mean \pm SD. P values were determined by unpaired two-tailed Student's *t* test. * $P < 0.05$; ** $P < 0.01$; and *** $P < 0.001$.

antigens from the intestine. Moreover, *Ewsr1*^{BKO} mice did not show any autoimmune symptoms in our observation (up to 12 mo), suggesting that inhibition of this pathway only enhances pathogen-specific antibody responses but not autoimmune anti-body responses.

In conclusion, our findings establish the TRAF3–EWSR1 signaling axis as a checkpoint for Bcl6 expression and GC response. The TRAF3–EWSR1 signaling axis is unique because it negatively controls induced GC formation and T cell-dependent IgG responses. These unique functions of the TRAF3–EWSR1 signaling axis make it a potential target that could help clinicians

accurately modulate the immune response to treat challenging or emerging infectious diseases.

Materials and methods

Mice

Ewsr1-flox strain recovery from frozen sperm was provided by The Centre for Phenogenomics. *Ewsr1*-flox mice (C57BL/6 background) were generated using a *loxP* system targeting exon 4 of the *Ewsr1* gene. The *Ewsr1*-flox mice were crossed with *Mbl*-Cre mice (C57BL/6 background, Jackson Laboratory)

to generate *Ewsr1* B cell–conditional KO (BKO, *Ewsr1^{fl/fl} Mbl-Cre*) and WT control (*Mbl-Cre* or *Ewsr1^{fl/fl}*) mice. In some experiments, *Ewsr1^{fl/fl} Mbl-Cre* mice were further crossed with *C3^{-/-}* mice (C57BL/6 background, Jackson Laboratory) or *Bcl6^{fl/fl}* mice (C57BL/6 background, Jackson Laboratory) to generate double-mutant mice. The *Traf3*-flox mice were crossed with *Mbl-Cre* or *Ewsr1^{+/+} Mbl-Cre* mice to generate *Traf3* B cell–conditional knockout (BKO, *Traf3^{fl/fl} Mbl-Cre*) or double knockout mice. ER26Stop^{FL}*Map3k14*, a *Map3k14*-bearing transgene encoding WT NIK under the control of a loxP-flanked STOP cassette (Sasaki et al., 2008), was crossed with *Mbl-Cre* mice to generate B cell–specific overexpression NIK mice (Btg, *Map3k14^{ts}Mbl-Cre*). The mice used in this study were co-caged and sex- and age-matched littermates, unless otherwise stated. Genotyping PCR was performed using the primers listed in Table S1. The animals used in this study were treated in accordance with relevant institutional and national guidelines and regulations. The use of animals in this study was approved by the institutional animal care and use committee of the Xiamen University and the University of Texas MD Anderson Cancer Center.

Plasmids

The pcDNA expression vectors encoding HA-tagged EWSR1 and its truncation mutants (EWSR1 [1–655], EWSR1 [1–30], and EWSR1 [300–655]) were created by PCR using human EWSR1 template and subcloned into the pcDNA-HA vector. Plasmid encoding HA-tagged TRAF3 and its truncation mutants were as described (Liao et al., 2004). pcDNA3.1 His-GFP-EWSR1-myc-His was purchased from Addgene (# 46385; plasmid). Primers used in the cloning experiment are listed in Table S1.

Antibodies and reagents

Fluorescence-labeled antibodies PE Hamster anti-mouse CD55 (RIKO-5), PE mouse anti-Bcl-6 (K112-91), APC rat anti-mouse CD184 (2B11), and PE rat anti-mouse IgG1 (A85-1) were purchased from BD Pharmingen. APC anti-mouse CD106 (429) and PE anti-mouse CD31 (390) were purchased from Biolegend. FITC anti-mouse CD21/CD35 (4E3) and PE anti-mouse CD38 (90) were purchased from eBioscience. Antibodies for TRAF3 (H-122, 1:1,000), RelB (C-19, 1:1,000), EWSR1 (B-1, 1:1,000), and Lamin B (C-20, 1:1,000) were purchased from Santa Cruz Biotechnology. Antibodies for p100/p52 (4,882, 1:1,000) were purchased from Cell Signaling Technology Inc. NP-KLH, NP-Ficolin, and NP-BSA were purchased from Biosearch Technologies. Other antibodies and reagents were as described (Li et al., 2019).

Cell culture and stimulation

Splenic B cell purification, HEK-293 cell culture, and transfection were as described (Li et al., 2019).

Immunoblot and IP

Whole-cell extracts or subcellular extracts were prepared for immunoblotting or IP as described (Li et al., 2019).

RNA-seq

For bulk RNA-seq experiments, PP cells from WT and *Ewsr1^{BKO}* mice were isolated from the small intestine and stained for

15 min with anti-B220 PerCP-Cy5.5, anti-Fas FITC, anti-GL7 PB antibodies at 4°C. GC B cells (B220⁺ Fas⁺GL7⁺) were sorted on a FACSAria sorter (BD Biosciences). Total RNA was isolated using QIAGEN-RNeasy Micro Kit and subjected to RNA-seq using an Illumina sequencer. The raw reads are aligned to the Mouse reference genome (mm10) using Star RNASeq alignment software. HTseq is used to summarize the gene expression counts from the mapped BAM files. The raw counts are normalized and differential expression analysis is performed on protein-coding genes using the R package DESeq2. P-values obtained after multiple tests were adjusted for using the Benjamini-Hochberg method. Significant differentially expressed genes are defined by $P < 0.05$. GSEA was performed on RNA-seq data using GSEA 2.2.0 with gene randomization (Subramanian et al., 2005).

For scRNA-seq experiments, PP cells from WT and *Ewsr1^{BKO}* mice (three 8-wk-old male mice mixed together as one sample for each group) were stained for 15 min with anti-CD45 FITC, anti-CD19 APC antibodies, and Dead marker (propidium iodide) for live dead discrimination. Viable B cells (CD45⁺CD19⁺Dead⁻) were sorted on a FACSAria sorter. Single-cell suspensions were assessed for cell concentration and viability using Life Technologies Countess 3 FL cell counter using 0.4% trypan blue exclusion staining. Samples passing QC fall in the concentration range for their cell target capture and have a viability of at least 70% or higher. Reagents, consumables, reaction master mixes, reaction volumes, cycling numbers, cycling conditions, and clean-up steps were completed following 10 × Genomics' 3' scRNA-seq V3.1 protocol. Quality control steps after cDNA amplification and library preparation steps were carried out by running Thermo Fisher Scientific Qubit HS dsDNA Assay along with Agilent HS DNA for concentration and quality assessments. Equal amounts of each uniquely indexed sample library were pooled together. The resultant pool was verified for concentration via qPCR using a KAPA Biosystems KAPA Library Quantification Kit. The pool was sequenced using a NovaSeq6000 sequencer and S Prime flow cell. The run parameters used were 28 cycles for read 1, 91 cycles for read 2, 8 cycles for index1, and 0 cycles for index2 as stipulated in the protocol mentioned above. Sample demultiplexing, barcode processing, alignment, filtering, unique molecular identifier counting, and aggregation of sequencing runs were performed using Cell Ranger analysis pipeline (v.5.0.0). Downstream analyses were performed in R using the Seurat package (v.4.0.1). Cells in which <200 and >3,000 gene expression, and in which mitochondrially encoded transcripts constituted more than 10% of the total library were excluded from downstream analysis. Each gene expression measurement was normalized by total expression in corresponding cell and multiplied by a scaling factor of 10,000. 2,000 high variable genes were used for principal component analysis. Principal components were determined to be significant ($P < 0.01$) using JackStraw method, t-distributed stochastic neighbor embedding was performed on the significant principle components using first 10 principal components, and the resolution was set as 0.2 for visualization in two dimensions. Unsupervised clustering was performed using Louvain algorithm (default). Differential expression analysis was performed between each

cluster and all other cells using a non-parametric Wilcoxon rank sum test. Top 10 enriched genes in each cluster were used to make a heatmap. CD19 subset was first identified and then reanalyzed by using procedure as mentioned above. CD19 cluster percentage was calculated and plotted using ggplot2 package in R. Gene expression data have been deposited in the Gene Expression Omnibus (GEO) public database with accession number GSE225103.

ChIP-seq analysis and CHIP-PCR

EWSR1 ChIP-seq data were downloaded from GEO with accession number GSE94275 (datasets GSE2472081 and GSE2472082). We evaluated the quality of raw reads and trimmed adaptors and low-quality reads using Trimmomatic (Bolger et al., 2014). High-quality reads were mapped to a reference genome (GRCh37) using bowtie2 with the end-to-end mode (Langmead and Salzberg, 2012). Reads with ≤ 3 mismatches and mapping quality score ≥ 20 were retained. PCR duplicates were removed using SAMtools (Li et al., 2009). Peak calling was performed with MACS2 (Zhang et al., 2008), compared with input control with false discovery rate < 0.05 . Deeptools (Ramírez et al., 2016) bamCoverage was used to convert bam to coverage normalized with library size and IGV was used for peak visualization (Robinson et al., 2011). ChIP assay was performed using the EpiQuik ChIP Kit (EpiGentek) and Hemagglutinin/HA (Roche) antibodies used for Chip-IP in BJAB cells transfected with control or HA-EWSR1. The precipitated and purified DNA was then quantified by qPCR using specific primers that amplify the BCL6 first intron (Table S1).

Microbiome analysis

16S ribosomal RNA gene sequencing was performed at the Alkek Center for Metagenomics and Microbiome Research, Baylor College of Medicine, as previously described (Jie et al., 2018). The mutant and WT mice were separately housed in this experiment.

Mouse model of *C. rodentium* oral infection

Mouse model of *C. rodentium* oral infection was performed as described previously (Jie et al., 2018). Briefly, Inoculate *C. rodentium* strain DBS100 (51459; ATCC) in 5 ml Luria-Bertani broth and culture it at 37°C, 200 rpm overnight. The concentration of bacteria was measured by checking OD at 600 nm and further confirmed as CFUs by smearing on Luria-Bertani agar plates after serial dilution. For oral gavage, each mouse was administered 5×10^9 CFUs of bacteria in a total volume of 300 μ l. To generate immune serum, WT or *Ewsr1*^{BKO} mice were infected orally with 5×10^9 CFUs of bacteria and the sera were collected 3 wk later. IgG-depleted immune serum was prepared by 1:2 diluting immune serum with binding buffer (20 mM sodium phosphate, pH 8.0) and then incubation with protein A/G agarose (Santa Cruz Biotechnology). For passive immunization, WT mice were infected orally with 5×10^9 CFUs of bacteria and treated on days 4–7 and 11–14 with 50 μ l of immune serum or 100 μ l IgG-depleted immune serum by intraperitoneal injection.

Histology and immunohistochemical staining

Fresh isolated colon was fixed in Bouin's solution (Sigma-Aldrich) for 1 h at room temperature. Fixed tissues were dehydrated by gradually soaking in ethanol (70, 80, 90, 95, and 100%) and xylene, and then embedded in paraffin. The paraffin-embedded tissues were cut into 5 μ m sections and stained with H&E. Pictures were taken with a digital inverted light microscope (EVOS; Thermo Fisher Scientific).

Immunohistochemical staining was performed on splenic tissue sections. Briefly, the sections were subjected to heat-induced antigen retrieval by incubation in 0.01 M sodium citrate buffer (pH 6.0) at 98°C for 10 min. After washing with PBS, the sections were blocked with normal goat serum (#KIT-9710; MXB) at room temperature for 1 h. The sections were then incubated overnight at 4°C with biotinylated peanut agglutinin (1:250, Vector Laboratories). After washing for 30 min with PBS, the sections were developed with 3,3'-diaminobenzidine substrate (#SK-4100; Vector Laboratories) and counterstained with hematoxylin. Finally, the sections were dehydrated and mounted with a coverslip. The presence of germinal center was visualized as brown staining in the sections under a microscope.

RT-qPCR

Total RNA preparation and RT-qPCR were as described previously (Li et al., 2016). The relative expression of the indicated genes was calculated using a standard curve method and was normalized to the expression of *Actb*. The primers used in RT-qPCR assays are shown in Table S1.

Mouse immunization, feces homogenization, and ELISA

Age-matched WT and *Ewsr1*^{BKO} mice were injected intraperitoneally with 0.2 ml NP-KLH or NP-Ficoll (0.1 mg/ml in PBS). On days 0 (unimmunized), 4, 7, 14, serum was collected from peripheral blood, and NP-specific antibodies were analyzed by ELISA (Southern Biotech).

Fresh feces were collected from individual mice, weighed, and homogenized in sterile PBS containing 1% (wt/vol) sodium azide and protease inhibitor mix. ELISA was used to detect the different isotopes of antibodies (Southern Biotech).

Statistical analysis

Statistical analysis was performed using GraphPad Prism software. Significant changes between the two groups were analyzed with an unpaired two-tailed Student's *t* test. P values < 0.05 were considered significant and the level of significance was indicated as **P* < 0.05 , ***P* < 0.01 , and ****P* < 0.001 .

Online supplemental material

The online supplementary information describes the generation of *Ewsr1*^{BKO} mice (Fig. S1), the impact of EWSR1 knockout on B cell development (Fig. S2), detailed analysis of WT, *C3*^{-/-}, *Ewsr1*^{BKO}, and *C3*^{-/-}*Ewsr1*^{BKO} mice (Fig. S3), detailed information on scRNA-seq analysis (Fig. S4), commensal microbiota analysis in the fecal extracts of WT and *Ewsr1*^{BKO} mice (Fig. S5), sequences of oligonucleotide primers used in this study (Table S1), details information on RNA-seq analysis (Table S2), and uncropped

gel pictures corresponding to Western blots shown in Fig. 2, Fig. 6, and Fig. S1 (source data files).

Acknowledgments

This study was supported by grants from the National Key R&D Program of China (2021YFC2701800, 2021YFC2701802 to Z. Jie), the National Natural Science Foundation of China (32170902 to Z. Jie, 81872114 to S. Zhao), the Fundamental Research Funds for the Central Universities (20720210113 and 20720220003 to Z. Jie), and the Jiangsu Provincial Special Program of Medical Science (BE2019617 to S. Zhao).

Author contributions: Y. Li designed and performed the research, prepared the figures, and wrote the manuscript; L. Zhu, C.-J. Ko, J.-Y. Yang, H. Wang, and X. Cheng contributed experiments; G. Manyam and J. Wang contributed to the sequencing data analysis; S. Zhao provided essential mouse models, scientific advice, and contributed to the experiments; Z. Jie provided essential mouse models, designed the research, and wrote the manuscript.

Disclosures: The authors declare no competing interests exist.

Submitted: 29 August 2022

Revised: 29 December 2022

Accepted: 20 March 2023

References

Araya, N., K. Hirota, Y. Shimamoto, M. Miyagishi, E. Yoshida, J. Ishida, S. Kaneko, M. Kaneko, T. Nakajima, and A. Fukamizu. 2003. Cooperative interaction of EWS with CREB-binding protein selectively activates hepatocyte nuclear factor 4-mediated transcription. *J. Biol. Chem.* 278: 5427–5432. <https://doi.org/10.1074/jbc.M210234200>

Arkatkar, T., S.W. Du, H.M. Jacobs, E.M. Dam, B. Hou, J.H. Buckner, D.J. Rawlings, and S.W. Jackson. 2017. B cell-derived IL-6 initiates spontaneous germinal center formation during systemic autoimmunity. *J. Exp. Med.* 214:3207–3217. <https://doi.org/10.1084/jem.20170580>

Aurias, A., C. Rimbaut, D. Buffe, J. Dubouset, and A. Mazabraud. 1983. Translocation of chromosome 22 in Ewing's sarcoma. *C. R. Seances Acad. Sci. III.* 296:1105–1107.

Basso, K., and R. Dalla-Favera. 2010. BCL6: Master regulator of the germinal center reaction and key oncogene in B cell lymphomagenesis. *Adv. Immunol.* 105:193–210. [https://doi.org/10.1016/S0065-2776\(10\)05007-8](https://doi.org/10.1016/S0065-2776(10)05007-8)

Beccaria, C.G., M.C. Amezcua Vesely, F. Fiocca Vernengo, R.C. Gehrau, M.C. Ramello, J. Tosello Boari, M. Gorosito Serrán, J. Mucci, E. Piaggio, O. Campetella, et al. 2018. Galectin-3 deficiency drives lupus-like disease by promoting spontaneous germinal centers formation via IFN- γ . *Nat. Commun.* 9:1628. <https://doi.org/10.1038/s41467-018-04063-5>

Bertolotti, A., T. Melot, J. Acker, M. Vigneron, O. Delattre, and L. Tora. 1998. EWS, but not EWS-FLI-1, is associated with both TFIID and RNA polymerase II: Interactions between two members of the TET family, EWS and hTAFII68, and subunits of TFIID and RNA polymerase II complexes. *Mol. Cell. Biol.* 18:1489–1497. <https://doi.org/10.1128/MCB.18.3.1489>

Bolger, A.M., M. Lohse, and B. Usadel. 2014. Trimmomatic: A flexible trimmer for Illumina sequence data. *Bioinformatics.* 30:2114–2120. <https://doi.org/10.1093/bioinformatics/btu170>

Boulay, G., G.J. Sandoval, N. Riggi, S. Iyer, R. Buisson, B. Naigles, M.E. Awad, S. Rengarajan, A. Volorio, and M.J. McBride. 2017. Cancer-specific re-targeting of BAF complexes by a prion-like domain. *Cell.* 171:163–178. e119. <https://doi.org/10.1016/j.cell.2017.07.036>

Caballero-Flores, G., K. Sakamoto, M.Y. Zeng, Y. Wang, J. Hakim, V. Matus-Acuña, N. Inohara, and G. Núñez. 2019. Maternal immunization confers protection to the offspring against an attaching and effacing pathogen through delivery of IgG in breast milk. *Cell Host Microbe.* 25:313–323. e314. <https://doi.org/10.1016/j.chom.2018.12.015>

Cherukuri, A., P.C. Cheng, H.W. Sohn, and S.K. Pierce. 2001. The CD19/CD21 complex functions to prolong B cell antigen receptor signaling from lipid rafts. *Immunity.* 14:169–179. [https://doi.org/10.1016/S1074-7613\(01\)00098-X](https://doi.org/10.1016/S1074-7613(01)00098-X)

Cumpelik, A., D. Heja, Y. Hu, G. Varano, F. Ordikhani, M.P. Roberto, Z. He, D. Homann, S.A. Lira, D. Dominguez-Sola, and P.S. Heeger. 2021. Dynamic regulation of B cell complement signaling is integral to germinal center responses. *Nat. Immunol.* 22:757–768. <https://doi.org/10.1038/s41590-021-00926-0>

Cyster, J.G., and C.D.C. Allen. 2019. B cell responses: Cell interaction dynamics and decisions. *Cell.* 177:524–540. <https://doi.org/10.1016/j.cell.2019.03.016>

Dent, A.L., A.L. Shaffer, X. Yu, D. Allman, and L.M. Staudt. 1997. Control of inflammation, cytokine expression, and germinal center formation by BCL-6. *Science.* 276:589–592. <https://doi.org/10.1126/science.276.5312.589>

Domeier, P.P., S.B. Chodiseti, C. Soni, S.L. Schell, M.J. Elias, E.B. Wong, T.K. Cooper, D. Kitamura, and Z.S. Rahman. 2016. IFN- γ receptor and STAT1 signaling in B cells are central to spontaneous germinal center formation and autoimmunity. *J. Exp. Med.* 213:715–732. <https://doi.org/10.1084/jem.20151722>

Domeier, P.P., S.L. Schell, and Z.S. Rahman. 2017. Spontaneous germinal centers and autoimmunity. *Autoimmunity.* 50:4–18. <https://doi.org/10.1080/08916934.2017.1280671>

El Shikh, M.E.M., R.M. El Sayed, S. Sukumar, A.K. Szakal, and J.G. Tew. 2010. Activation of B cells by antigens on follicular dendritic cells. *Trends Immunol.* 31:205–211. <https://doi.org/10.1016/j.it.2010.03.002>

Fukuda, T., T. Yoshida, S. Okada, M. Hatano, T. Miki, K. Ishibashi, S. Okabe, H. Koseki, S. Hirose, M. Taniguchi, et al. 1997. Disruption of the Bcl6 gene results in an impaired germinal center formation. *J. Exp. Med.* 186: 439–448. <https://doi.org/10.1084/jem.186.3.439>

Han, S., K. Hathcock, B. Zheng, T.B. Kepler, R. Hodes, and G. Kelsoe. 1995. Cellular interaction in germinal centers. Roles of CD40 ligand and B7-2 in established germinal centers. *J. Immunol.* 155:556–567. <https://doi.org/10.4049/jimmunol.155.2.556>

Jie, Z., J.-Y. Yang, M. Gu, H. Wang, X. Xie, Y. Li, T. Liu, L. Zhu, J. Shi, L. Zhang, et al. 2018. NIK signaling axis regulates dendritic cell function in intestinal immunity and homeostasis. *Nat. Immunol.* 19: 1224–1235. <https://doi.org/10.1038/s41590-018-0206-z>

Kamada, N., K. Sakamoto, S.-U. Seo, M.Y. Zeng, Y.-G. Kim, M. Cascalho, B.A. Vallance, J.L. Puente, and G. Núñez. 2015. Humoral immunity in the gut selectively targets phenotypically virulent attaching-and-effacing bacteria for intraluminal elimination. *Cell Host Microbe.* 17:617–627. <https://doi.org/10.1016/j.chom.2015.04.001>

Kerfoot, S.M., G. Yaari, J.R. Patel, K.L. Johnson, D.G. Gonzalez, S.H. Kleinstein, and A.M. Haberman. 2011. Germinal center B cell and T follicular helper cell development initiates in the interfollicular zone. *Immunity.* 34: 947–960. <https://doi.org/10.1016/j.immuni.2011.03.024>

Kikuchi, M., T. Miki, T. Kumagai, T. Fukuda, 2015. Humoral immunity in the gut selectively targets phenotypically virulent attaching-and-effacing bacteria for intraluminal elimination. *Cell Host Microbe.* 17:617–627. <https://doi.org/10.1016/j.chom.2015.04.001>

Kitano, M., S. Moriyama, Y. Ando, M. Hikida, Y. Mori, T. Kurosaki, and T. Okada. 2011. Bcl6 protein expression shapes pre-germinal center B cell dynamics and follicular helper T cell heterogeneity. *Immunity.* 34: 961–972. <https://doi.org/10.1016/j.immuni.2011.03.025>

Langmead, B., and S.L. Salzberg. 2012. Fast gapped-read alignment with Bowtie 2. *Nat. Methods.* 9:357–359. <https://doi.org/10.1038/nmeth.1923>

Lee, J., P.T. Nguyen, H.S. Shim, S.J. Hyeon, H. Im, M.-H. Choi, S. Chung, N.W. Kowall, S.B. Lee, and H. Ryu. 2019. EWSR1, a multifunctional protein, regulates cellular function and aging via genetic and epigenetic pathways. *Biochim. Biophys. Acta Mol. Basis Dis.* 1865:1938–1945. <https://doi.org/10.1016/j.bbdis.2018.10.042>

Li, H., B. Handsaker, A. Wysoker, T. Fennell, J. Ruan, N. Homer, G. Marth, G. Abecasis, R. Durbin, and 1000 Genome Project Data Processing Subgroup. 2009. The sequence alignment/map format and SAMtools. *Bioinformatics.* 25:2078–2079. <https://doi.org/10.1093/bioinformatics/btp352>

Li, Y., H. Wang, X. Zhou, X. Xie, X. Chen, Z. Jie, Q. Zou, H. Hu, L. Zhu, X. Cheng, et al. 2016. Cell intrinsic role of NF-kappaB-inducing kinase in regulating T cell-mediated immune and autoimmune responses. *Sci Rep.* 6:22115. <https://doi.org/10.1038/srep22115>

Li, Y., X. Xie, Z. Jie, L. Zhu, J.-Y. Yang, C.-J. Ko, T. Gao, A. Jain, S.Y. Jung, N. Baran, et al. 2021. DYRK1a mediates BAFF-induced noncanonical NF- κ B activation to promote autoimmunity and B-cell leukemogenesis. *Blood.* 138:2360–2371. <https://doi.org/10.1182/blood.2021011247>

- Li, Y., J.Y. Yang, X. Xie, Z. Jie, L. Zhang, J. Shi, D. Lin, M. Gu, X. Zhou, H.S. Li, et al. 2019. Preventing abnormal NF- κ B activation and autoimmunity by Otb1-mediated p100 stabilization. *Cell Res.* 29:474–485. <https://doi.org/10.1038/s41422-019-0174-3>
- Liao, G., M. Zhang, E.W. Harhaj, and S.C. Sun. 2004. Regulation of the NF- κ B-inducing kinase by tumor necrosis factor receptor-associated factor 3-induced degradation. *J. Biol. Chem.* 279:26243–26250. <https://doi.org/10.1074/jbc.M403286200>
- Lublin, D.M., and J.P. Atkinson. 1989. Decay-accelerating factor: Biochemistry, molecular biology, and function. *Annu. Rev. Immunol.* 7:35–58. <https://doi.org/10.1146/annurev.iy.07.040189.000343>
- Maaser, C., M.P. Housley, M. Imura, J.R. Smith, B.A. Vallance, B.B. Finlay, J.R. Schreiber, N.M. Varki, M.F. Kagnoff, and L. Eckmann. 2004. Clearance of *Citrobacter rodentium* requires B cells but not secretory immunoglobulin A (IgA) or IgM antibodies. *Infect. Immun.* 72:3315–3324. <https://doi.org/10.1128/IAI.72.6.3315-3324.2004>
- Masuda, A., M. Yoshida, H. Shiomi, S. Ikezawa, T. Takagawa, H. Tanaka, R. Chinzei, T. Ishida, Y. Morita, H. Kutsumi, et al. 2008. Fc γ receptor regulation of *Citrobacter rodentium* infection. *Infect. Immun.* 76:1728–1737. <https://doi.org/10.1128/IAI.01493-07>
- Nielsen, C.H., E.M. Fischer, and R.G. Leslie. 2000. The role of complement in the acquired immune response. *Immunology.* 100:4–12. <https://doi.org/10.1046/j.1365-2567.2000.00009.x>
- Ramírez, F., D.P. Ryan, B. Grüning, V. Bhardwaj, F. Kilpert, A.S. Richter, S. Heyne, F. Dündar, and T. Manke. 2016. deepTools2: a next generation web server for deep-sequencing data analysis. *Nucleic Acids Res.* 44:W160–5. <https://doi.org/10.1093/nar/gkw257>
- Robinson, J.T., H. Thorvaldsdóttir, W. Winckler, M. Guttman, E.S. Lander, G. Getz, and J.P. Mesirov. 2011. Integrative genomics viewer. *Nat. Biotechnol.* 29:24–26. <https://doi.org/10.1038/nbt.1754>
- Robinson, M.J., Z. Ding, C. Pitt, E.J. Brodie, I. Quast, D.M. Tarlinton, and D. Zotos. 2020. The amount of BCL6 in B cells shortly after antigen engagement determines their representation in subsequent germinal centers. *Cell Rep.* 30:1530–1541. e1534. <https://doi.org/10.1016/j.celrep.2020.01.009>
- Round, J.L., and S.K. Mazmanian. 2009. The gut microbiota shapes intestinal immune responses during health and disease. *Nat. Rev. Immunol.* 9:313–323. <https://doi.org/10.1038/nri2515>
- Saito, M., U. Novak, E. Piovan, K. Basso, P. Sumazin, C. Schneider, M. Crespo, Q. Shen, G. Bhagat, A. Califano, et al. 2009. BCL6 suppression of BCL2 via Miz1 and its disruption in diffuse large B cell lymphoma. *Proc. Natl. Acad. Sci. USA.* 106:11294–11299. <https://doi.org/10.1073/pnas.0903854106>
- Sasaki, Y., D.P. Calado, E. Derudder, B. Zhang, Y. Shimizu, F. Mackay, S. Nishikawa, K. Rajewsky, and M. Schmidt-Supprian. 2008. NIK overexpression amplifies, whereas ablation of its TRAF3-binding domain replaces BAFF:BAFF-R-mediated survival signals in B cells. *Proc. Natl. Acad. Sci. USA.* 105:10883–10888. <https://doi.org/10.1073/pnas.0805186105>
- Scholz, J.L., J.E. Crowley, M.M. Tomayko, N. Steinel, P.J. O'Neill, W.J. Quinn III, R. Goenka, J.P. Miller, Y.H. Cho, V. Long, et al. 2008. Bly5 inhibition eliminates primary B cells but leaves natural and acquired humoral immunity intact. *Proc. Natl. Acad. Sci. USA.* 105:15517–15522. <https://doi.org/10.1073/pnas.0807841105>
- Suan, D., N.J. Kräutler, J.L. Maag, D. Butt, K. Bourne, J.R. Hermes, D.T. Avery, C. Young, A. Statham, and M. Elliott. 2017. CCR6 defines memory B cell precursors in mouse and human germinal centers, revealing light-zone location and predominant low antigen affinity. *Immunity.* 47:1142–1153. e1144. <https://doi.org/10.1016/j.immuni.2017.11.022>
- Subramanian, A., P. Tamayo, V.K. Mootha, S. Mukherjee, B.L. Ebert, M.A. Gillette, A. Paulovich, S.L. Pomeroy, T.R. Golub, E.S. Lander, and J.P. Mesirov. 2005. Gene set enrichment analysis: A knowledge-based approach for interpreting genome-wide expression profiles. *Proc. Natl. Acad. Sci. USA.* 102:15545–15550. <https://doi.org/10.1073/pnas.0506580102>
- Sun, S.-C. 2017. The non-canonical NF- κ B pathway in immunity and inflammation. *Nat. Rev. Immunol.* 17:545–558. <https://doi.org/10.1038/nri.2017.52>
- Tan, A.Y., and J.L. Manley. 2009. The TET family of proteins: Functions and roles in disease. *J. Mol. Cell Biol.* 1:82–92. <https://doi.org/10.1093/jmcb/mjp025>
- Turner, J.S., J.A. O'Halloran, E. Kalaidina, W. Kim, A.J. Schmitz, J.Q. Zhou, T. Lei, M. Thapa, R.E. Chen, J.B. Case, et al. 2021. SARS-CoV-2 mRNA vaccines induce persistent human germinal centre responses. *Nature.* 596:109–113. <https://doi.org/10.1038/s41586-021-03738-2>
- Victoria, G.D., and M.C. Nussenzweig. 2022. Germinal centers. *Annu. Rev. Immunol.* 40:413–442. <https://doi.org/10.1146/annurev-immunol-120419-022408>
- Xie, P., L.L. Stunz, K.D. Larison, B. Yang, and G.A. Bishop. 2007. Tumor necrosis factor receptor-associated factor 3 is a critical regulator of B cell homeostasis in secondary lymphoid organs. *Immunity.* 27:253–267. <https://doi.org/10.1016/j.immuni.2007.07.012>
- Yoshida, N., D. Kitayama, M. Arima, A. Sakamoto, A. Inamine, H. Watanabe-Takano, M. Hatano, T. Koike, and T. Tokuhisa. 2011. CXCR4 expression on activated B cells is downregulated by CD63 and IL-21. *J. Immunol.* 186:2800–2808. <https://doi.org/10.4049/jimmunol.1003401>
- Young, C., and R. Brink. 2021. The unique biology of germinal center B cells. *Immunity.* 54:1652–1664. <https://doi.org/10.1016/j.immuni.2021.07.015>
- Zeng, M.Y., D. Cisalpino, S. Varadarajan, J. Hellman, H.S. Warren, M. Cascalho, N. Inohara, and G. Núñez. 2016. Gut microbiota-induced immunoglobulin G controls systemic infection by symbiotic bacteria and pathogens. *Immunity.* 44:647–658. <https://doi.org/10.1016/j.immuni.2016.02.006>
- Zhang, B., D.P. Calado, Z. Wang, S. Fröhler, K. Köchert, Y. Qian, S.B. Koralov, M. Schmidt-Supprian, Y. Sasaki, C. Unitt, et al. 2015. An oncogenic role for alternative NF- κ B signaling in DLBCL revealed upon deregulated BCL6 expression. *Cell Rep.* 11:715–726. <https://doi.org/10.1016/j.celrep.2015.03.059>
- Zhang, Y., T. Liu, C.A. Meyer, J. Eeckhoute, D.S. Johnson, B.E. Bernstein, C. Nusbaum, R.M. Myers, M. Brown, W. Li, and X.S. Liu. 2008. Model-based analysis of ChIP-seq (MACS). *Genome Biol.* 9:R137. <https://doi.org/10.1186/gb-2008-9-9-r137>

Supplemental material

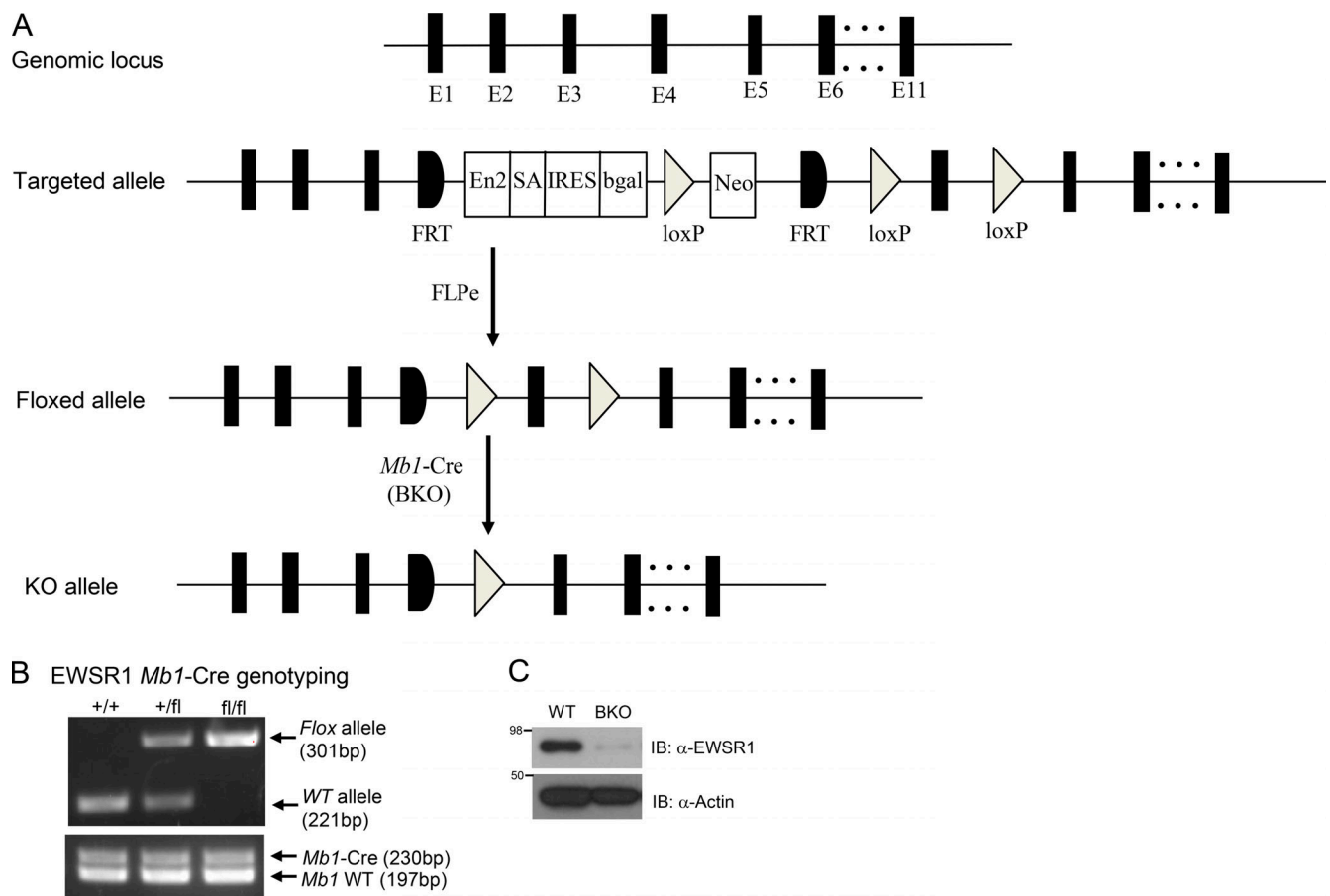


Figure S1. **Generation of *Ewsr1*^{BKO} mice.** (A) Schematic of *Ewsr1* gene targeting using an FRT-LoxP vector. Targeted mice were crossed with *Mb1-Cre* to generate BKO mice. (B) Genotyping PCR analysis of *Ewsr1*^{+/+} (+/+), *Ewsr1*^{+/fl} (+/fl), and *Ewsr1*^{fl/fl} (fl/fl) mice crossed with *Mb1-Cre* mice, showing WT and flox alleles of *Ewsr1* gene as well as *Mb1* WT and *Mb1-Cre* fusion gene locus. (C) Immunoblot (IB) analysis of the EWSR1 proteins deletion in whole-cell lysates of freshly isolated splenic B cells from WT and *Ewsr1*^{BKO} mice. Data are representative of three independent experiments. The molecular weight measurements are kD. Source data are available for this figure: SourceData FS1.

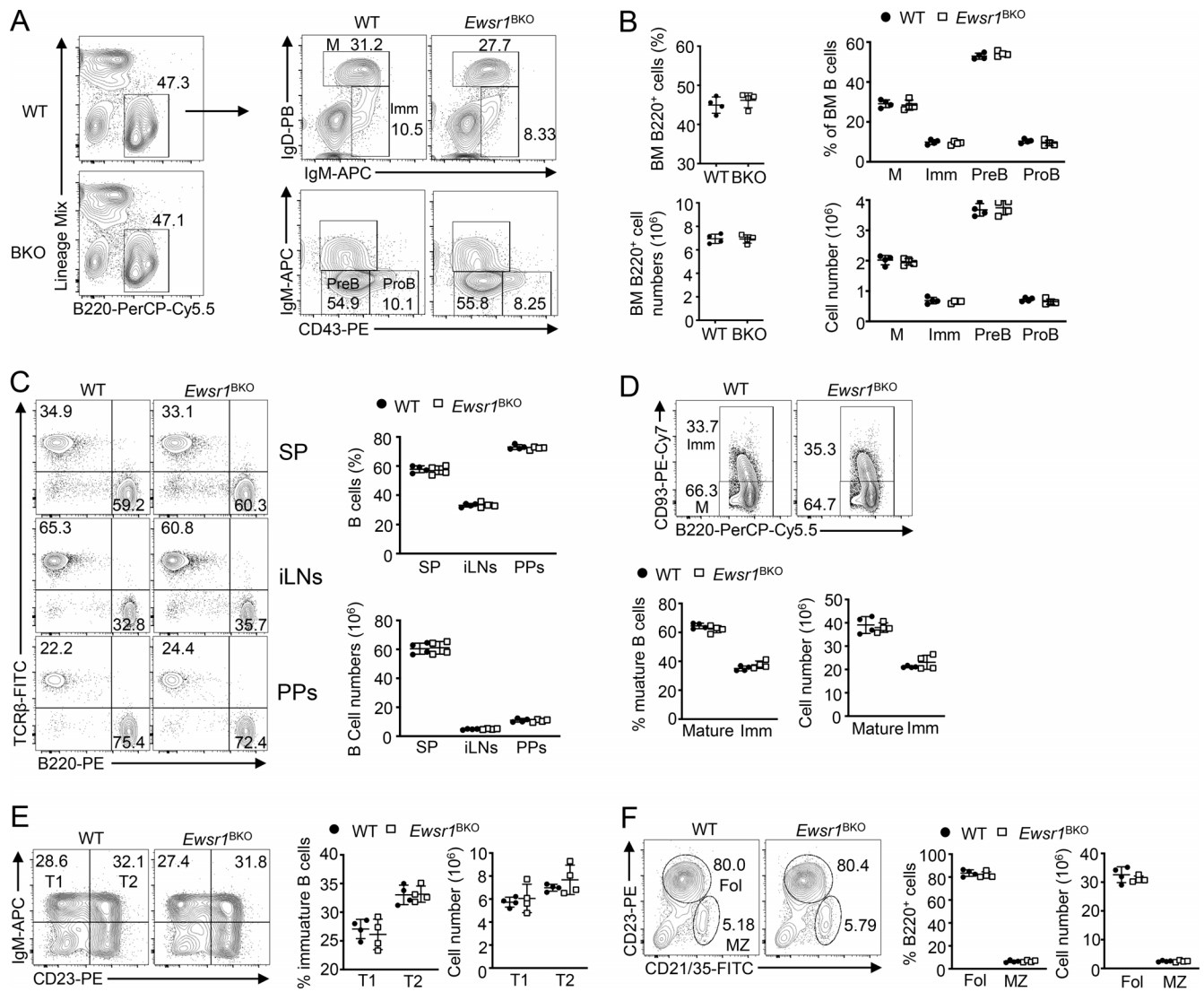


Figure S2. Flow cytometric analysis of B cell-specific EWSR1 deletion in bone marrow and secondary lymphoid organs. (A and B) Flow cytometric analysis of pro-B (B220⁺ IgM⁻CD43⁺), pre-B cell (B220⁺ IgM⁻CD43⁺), immature B (Imm, B220⁺ IgM⁺ IgD⁻), and mature B (M, B220⁺ IgM⁺ IgD⁺) stages in the bone marrow (BM) of WT and *Ewsr1*^{BKO} mice (*n* = 4 mice/group, 6–8 wk old). **(C)** Flow cytometric analyses of B220⁺ B cells in the spleen (SP), inguinal lymph nodes (iLNs), and PPs of WT or *Ewsr1*^{BKO} mice (*n* = 4 mice/group, 6–8 wk old). **(D–F)** Flow cytometric analyses of immature (Imm, B220⁺CD93⁺) and mature (B220⁺CD93⁻) B cells (D), immature T1 (CD93⁺IgM⁺CD23⁻) and T2 (CD93⁺IgM⁺CD23⁺) B cells (E), and follicular ([Fol] B220⁺CD21^{int}CD23⁺CD93⁻) and marginal zone ([MZ] B220⁺CD21^{hi}CD23⁻CD93⁻) B cells (F) in the spleens of WT and *Ewsr1*^{BKO} mice (*n* = 4 mice/group, 6–8 wk old). Data are representative of three independent experiments. Summary graphs are presented as mean ± SD, and P values were determined by unpaired two-tailed Student's *t* test.

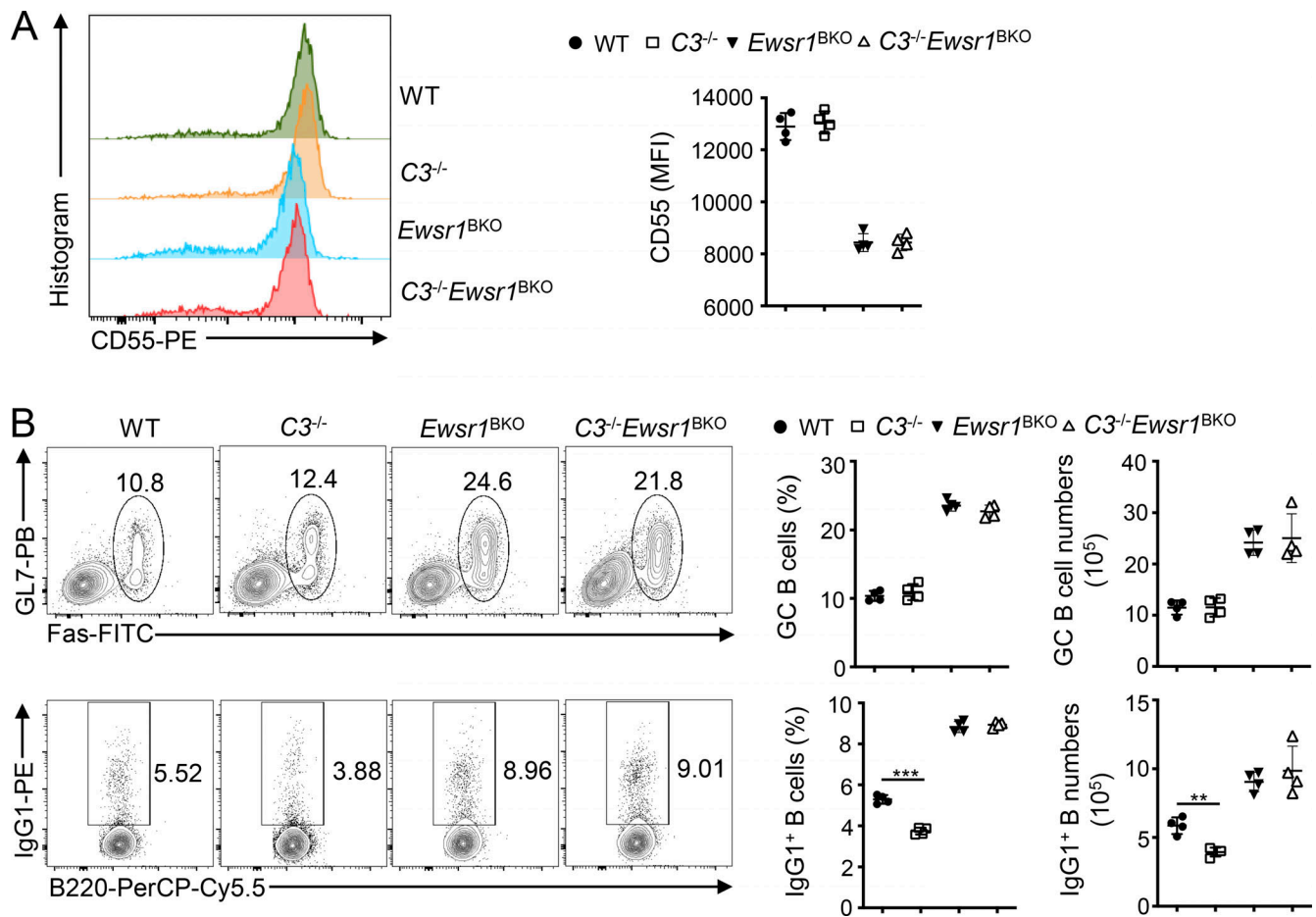


Figure S3. **Flow cytometric analysis of WT, $C3^{-/-}$, $Ewsr1^{BKO}$, and $C3^{-/-}Ewsr1^{BKO}$ mice.** (A) Flow cytometric analysis of the CD55 expression on gated splenic B cells from WT, $C3^{-/-}$, $Ewsr1^{BKO}$, and $C3^{-/-}Ewsr1^{BKO}$ ($n = 4$ mice/group, 6–8 wk old), presented as representative histograms (left) and summary graph of median fluorescence intensity (MFI; right). (B) Flow cytometric analyses of GC B cells and IgG1⁺ B cells in PPs of WT, $C3^{-/-}$, $Ewsr1^{BKO}$, and $C3^{-/-}Ewsr1^{BKO}$ ($n = 4$ mice/group, 6–8 wk old). Data are representative of two independent experiments. Summary graphs are presented as mean \pm SD, and P values were determined by unpaired two-tailed Student's *t* test. ** $P < 0.01$; and *** $P < 0.001$.

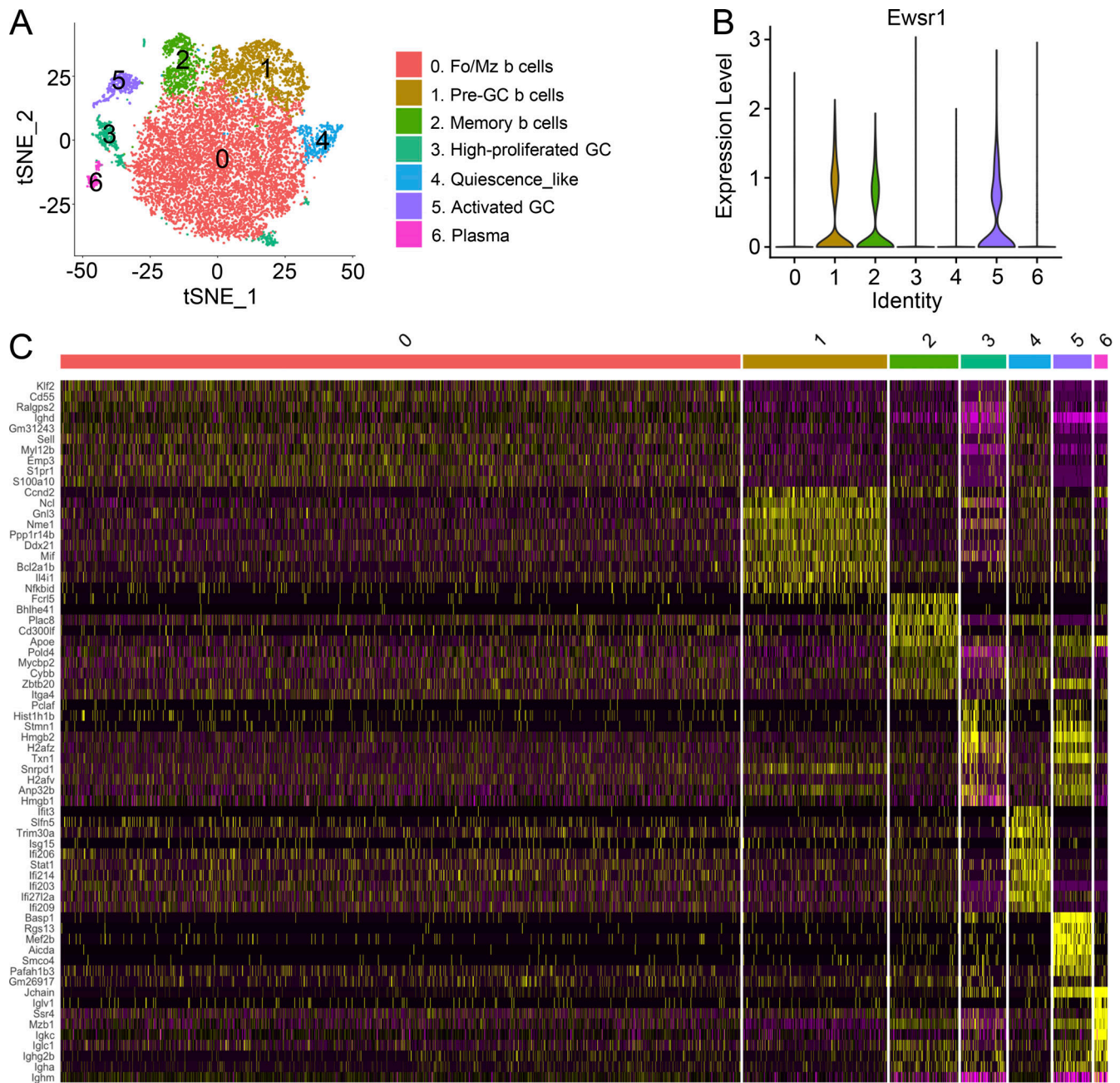


Figure S4. **scRNA-seq analysis of PPs B cells subsets in WT and *Ewsr1*^{BKO} mice.** (A) scRNA-seq data from WT and *Ewsr1*^{BKO} PP B cells were combined with batch correction for a total of 13,645 cells (shown as individual dots) and displayed by annotated t-distributed stochastic neighbor embedding (tSNE). FoI/MZ, follicular/marginal zone. (B) Violin plot showing the expression level of *Ewsr1* among B cell clusters in WT PP B cells. (C) Heatmap showing integrated scRNA-seq analysis of top differentially expressed genes between WT and *Ewsr1*^{BKO} mice in each identified cluster. Data are representative of one independent experiment.

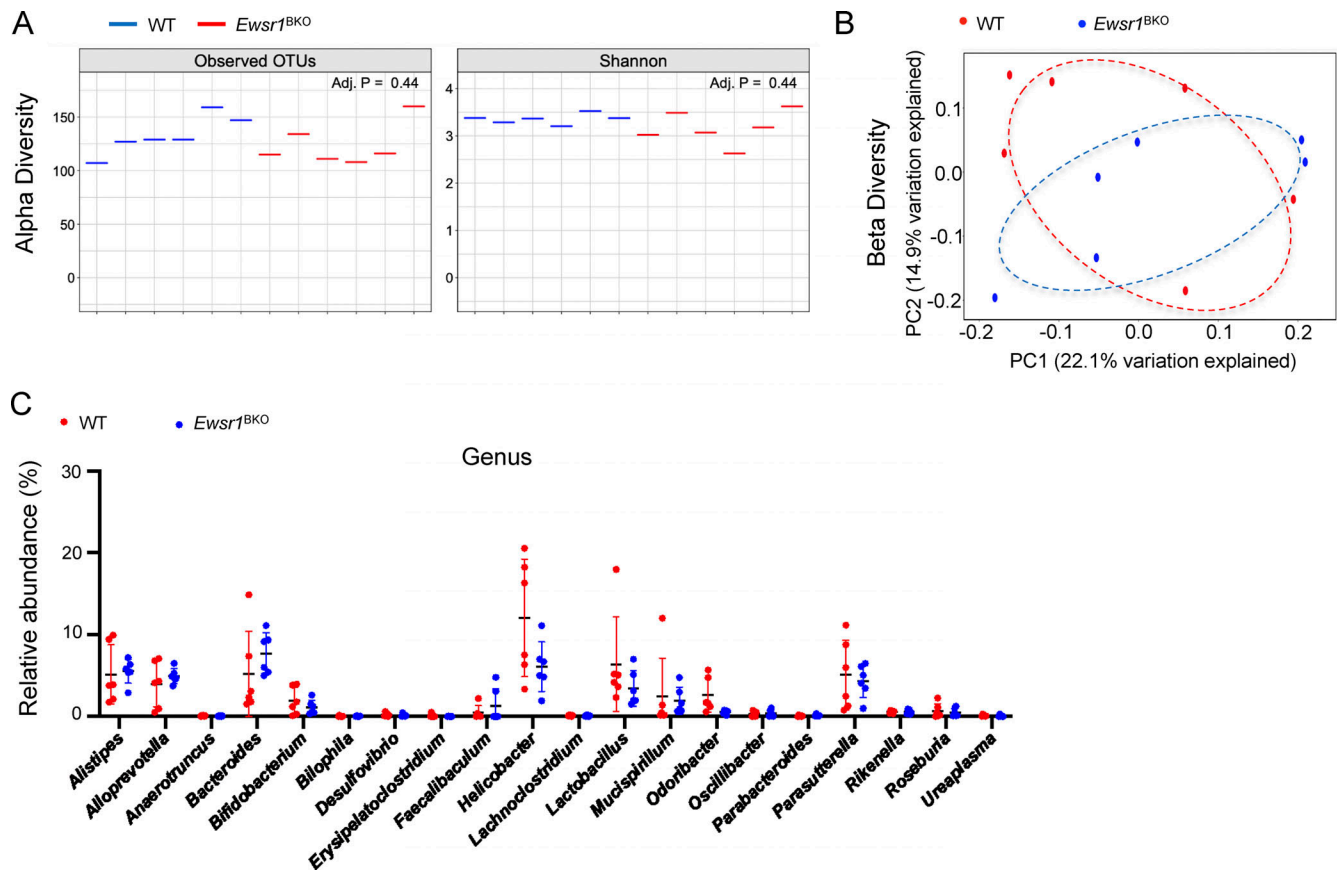


Figure S5. **Commensal microbiota analysis in the fecal extracts of WT and *Ewsr1^{BKO}* mice.** (A) Visualization of alpha diversity by principal coordinate analysis (PCoA). OTU, operational taxonomic units. (B) Visualization of beta diversity by PCoA. (C) Microbiota composition at genus level ($n = 6$ mice/group, 8 wk old male). Data are representative of one independent experiment.

Provided online are two tables. Table S1 shows gene-specific primers used in experiments. Table S2 shows details information on RNA-seq analysis.